Tobias Rye Torben

Control allocation and observer design for autonomous ferries

Master's thesis in Marine Technology
Supervisor: Asgeir J. Sørensen (Main) and Astrid H. Brodtkorb (Co)
August 2019

Master's thesis

NTNU
Norwegian University of Science and Technology
Faculty of Engineering
Department of Marine Technology

NTNU
Norwegian University of
Science and Technology

Tobias Rye Torben

Control allocation and observer design for autonomous ferries

Master's thesis in Marine Technology
Supervisor: Asgeir J. Sørensen (Main) and Astrid H. Brodtkorb (Co)
August 2019

Norwegian University of Science and Technology
Faculty of Engineering
Department of Marine Technology

NTNU
Norwegian University of
Science and Technology

NTNU Trondheim
Norwegian University of Science and Technology
Department of Marine Technology

MASTER THESIS IN MARINE CYBERNETICS

SPRING 2019

FOR

STUD. TECHN. TOBIAS R. TORBEN

Control allocation and observer design for autonomous ferries

Work description

Several recent initiatives exist related to autonomy in ferry operations. Transitioning from manual to automatic control introduces several challenges, and thus calls for new solutions. This thesis should investigate two topics related to control of autonomous ferries.

First, the control allocation problem should be investigated for double ended ferries with symmetric thruster configuration. These ferries normally have one azimuth thruster in each end. In transit, both thursters are oriented to produce a forward thrust. However, in a docking scenario this does not yield satisfactory performance, since the time to produce a reverse thrust is very high as one thruster needs to turn 180 degrees. Methods to address this challenge should be investigated, and a control allocation algorithm should be developed.

The second topic is observer design. A generic methodology for improved transient state estimation and control of linear time-varying systems using a hybrid resetting design should be investigated. This has important applications to autonomous ferries, as ferry operations include several transient phases. This also has applications to dynamic positioning (DP) systems where the transient behaviour of model-based observers is inadequate. Examples include DP in ice and gangway operations.

The thesis should consist of two scientific papers with a resume in front.

Scope of work

Resume:

- Introduce the ferry concept and their operation.
- Give an overview of modelling and control of marine surface vessels, with particular emphasis on observers and control allocation.
- Introduce the field of hybrid systems and describe the mathematical framework to be used in this thesis.
- Conduct a case study to with autonomous docking of a car ferry.

Paper one:

- Develop a control allocation algorithm for double ended ferries with symmetric thruster configuration.
- Evaluate the results using simulations and full scale experiments with the passenger ferry prototype milliAmpère.
- Co-authors Astrid H. Brodtkorb and Asgeir J. Sørensen

Paper two:

- Develop a methodology for state estimation and control of linear time-varying systems using a hybrid resetting approach.
- Give stability results using the hybrid dynamical systems framework of Goebel, Sanfelice and Teel.

- Evaluate the results for a dynamic positioning system using simulations and/or experimental results.
- Co-authors Roger Skjetne and Øivind K. Kjerstad

The report shall be written in English and edited as an article collection with a resume in front, in the format of a report. It is supposed that Department of Marine Technology, NTNU, can use the results freely in its research work, unless otherwise agreed upon, by referring to the student's work.

The thesis should be submitted within 15. November 2019.

Professor Asgeir J. Sørensen
Supervisor

Abstract

In the recent years, there has been high activity related to autonomy in ships. Due to the relatively low mission complexity of ferry operations, ferries make a good candidate for piloting the transition towards increased autonomy in ships. This thesis presents two novel components for an autonomous ferry control system.

The first component is a control allocation algorithm for double-ended ferries with symmetrical thruster configuration. This is a standard setup for car ferries, with one centered azimuth in each end. The allocation problem is formulated using the extended thrust representation. This results in a four dimensional constrained nonlinear optimization problem. Using the thrust configuration constraint, a reformulation of the optimization problem is proposed, reducing the problem to a nonlinear, bounded scalar optimization problem. For this class of problems, there exists fast and robust solvers. Next, cost functions and bound constraints are proposed. During manual docking of ferries, it is common to have the thrusters pointing in opposite directions, and giving each a mean thrust against each other. This gives faster response from commanded to produced forces. The novel control allocation algorithm can support this mode of operation using the proposed constraints and cost function. The algorithm is tested in a simulation study with a car ferry and in full-scale experiments with a passenger ferry. The results from simulation indicates reduced error between the commanded and produced forces compared to existing methods. The experimental results demonstrate good dynamic positioning performance when using the novel control allocation algorithm. Comparing the computational complexity to a quadratic programming approach, the novel algorithm is, on average, 37.8 times faster, with a more narrow distribution of run times. This is a desired property in a real-time control system.

The second component is a resetting observer. The observer is applicable to generic linear time-varying systems and has particularly interesting applications for dynamic positioning of marine surface vessels. The motivation for designing a resetting observer is better handling of unmodelled dynamics and reactiveness to external disturbances without compromising steady-state performance. The continuous-time estimates are calculated from a Luenberger observer. A reset is triggered if the output estimation error exceeds predefined bounds. The new state estimates after a jump is calculated using a finite-time observer approach. The finite-time observer equations are derived for linear time-varying systems, and a method for online calculation of the state transition matrix is presented. The resetting observer equations are formulated in a hybrid dynamical systems framework, and sufficient conditions for Uniform Global pre-Asymptotic Stability are given. A case study is conducted for dynamic positioning of an offshore support vessel. Open-loop results show promising performance with improved transient performance when subject to an external disturbance.

Finally, a high-fidelity simulation study is performed, using both the control allocation and resetting observer in an autonomous docking operation for a car ferry. The simulation results show good performance, building confidence in the usability of the new components in an autonomous ferry control system.

Sammendrag

De siste årene har det vært høy aktivitet knyttet til autonomi i skip. Grunnet relativt lav operasjonskompleksitet, utgjør bilferger en god kanditat for å drive utviklingen mot økt autonomi i skip. Denne avhandlingen presenterer to komponenter for kontrollsystemet til en autonom ferge.

Den første komponenten er en kontrollallokasjonsalgoritme for baug-hekk symmetriske ferger med symmetrisk thrusteroppsett. Dette er et standard design for bilferger, med en sentrert azimuth-thruster i hver ende. Allokeringproblemet blir formulert ved hjelp av utvidet thrust representasjonen, som resulterer i et fire-dimensjonalt begrenset ulineært optimaliseringproblem. Ved å bruke thrustkonfigurasjonsbegrensningen foreslås en reformulering av optimaliseringsproblemet. Dette reduserer problemet til et ulineært bunded skalart optimaliseringsproblem. For denne typen problem finnes det raske og robuste løsere. Videre foreslås kostfunksjoner og begrensninger. Når en ferge legger til kai manuelt er det vanlig å snu thrusterne slik at de peker mot hverandre. Dette gir raskere respons fra ønsket kraft til produsert kraft. Den nye kontrollallokasjonsalgoritmen støtter denne måten å styre thrusterne på ved å bruke den foreslåtte kostfunksjonen og begrensningen. Algoritmen er testet i et simuleringsstudie med en bilferge og i fullskala eksperiment med en passasjerferge. Resultatene fra simuleringen indikerer mindre feil mellom ønsket og produsert kraft sammenlignet med eksisterende metoder. De eksperimentelle resultatene viser god ytelse for dynamisk posisjonering når den nye kontrolallokasjonsalgoritmen brukes. Ved å sammenligne kjøretiden til den nye algoritmen med en kvadratisk programmerings metode viser resultatene at den nye er 37.8 ganger raskere, i gjennomsnitt. Den har også en smalere fordeling av kjøretider, som er en ettertraktet egenskap for bruk i et sanntidskontrollsystem.

Den andre komponenten er en resettende tilstandsestimator. Tilstandsestimatoren kan brukes for generiske lineære tidsvariende system, men har særlig interessante anvendelser for dynamisk posisjonering av marine overflatefartøy. Motivasjonen for å utvikle en resettende tilstandsestimator er bedre håndtering av umodellert dynamikk og reaktivitet for eksterne forstyrrelser uten å gå på bekostning av ytelsen ved steady-state. Tilstandsestimatene i kontinuerlig tid beregnes fra en Luenberger tilstandsestimator. Et resett utløses dersom estimeringsfeilen overskrider forhåndsdefinerte grenser. Det nye tilstandsestimatet beregnes fra en tilstandsestimator som konvergerer i endelig tid (finite-time observer). Ligningene for en tilstandsestimator som konvergerer i endelig tid for et lineært tidsvarierende system utledes, og en metode for å beregne trasisjonsmatrisene online presenteres. Den resettende tilstandsestimatoren formuleres i et rammeverk for hybride dynamiske systemer, og tilstrekkelige betingelser for Uniform Global pre-Asymptotisk Stabilitet gis. Et case-studie gjennomføres for dynamisk posisjonering av et offshore supply fartøy. Åpen-løkke-resultater viser lovende ytelse med forbedret transient ytelse når skipet utsettes for en ekstern forstyrrelse.

Til slutt gjøres et simuleringsstudie hvor både kontrollallokasjonsalgoritmen og den resettende tilstandsestimatoren testes sammen i kontrollsystemet til en bilferge som legger til kai automatisk. Simuleringsresultatene viser god ytelse. Dette gir økt tiltro til deres bruk i kontrollsystemet til en autonom ferge.

Preface

This master thesis is written as the final part of my MSc degree in Marine Cybernetics at the department of Marine Technology at the Norwegian University of Science and Technology (NTNU) in Trondheim.

The thesis is also part of my integrated PhD programme in the project *Online Risk Management and Risk Control for Autonomous Ships* (ORCAS), which is funded by the Research Council of Norway through a KPN project and NTNU Centre for Autonomous Marine Operations and Systems (AMOS) through the Centres of Excellence funding scheme.

Being a stepping stone towards a PhD degree, this thesis is edited as a collection of scientific papers with a resume in front. The first paper, with title *Control allocation for double-ended ferries with full-scale experimental results*, is accepted for publication at the 2019 Control Applications for Marine Systems (CAMS 2019) conference. The second paper, with title *A resetting observer for LTV systems with application to dynamic positioning of marine surface vessels*, is a draft paper to be submitted to the 2020 American Control Conference (ACC 2020).

Until the papers are published, this thesis is for limited circulation only.

Acknowledgements

Several people have contributed to the completion of this thesis. First of all, I would like to thank my main supervisor, Professor Asgeir J. Sørensen, for being a continuous source of motivation and encouragement and for giving valuable feedback throughout the semester. I would also like to thank my co-supervisor and co-author of Paper 1, Astrid H. Brodtkorb, for giving highly detailed and constructive feedback to Paper 1 and scientific writing in general.

I am also grateful to my co-authors of Paper 2, Professor Roger Skjetne and Øivind K. Kjerstad for approaching me with the idea of a resetting observer methodology, and for close collaboration in the development of the final observer and in writing the report.

Without all of you, this thesis would not have been the same.

Acronyms

AD	Analog-to-digital
DA	Digital-to-analog
DOF	Degree of Freedom
DP	Dynamic Positioning
EKF	Extended Kalman Filter
GES	Globally Exponentially Stable
GNSS	Global Navigation Satelite System
GpAS	Globally pre-Asymptotically Stable
ILOS	Integral Line-of-sight
IMU	Inertial Measurement Unit
INS	Inertial Navigation System
LB	Locally Bounded
LOS	Line-of-sight

LQR	Linear Quadratic Regulator
LTV	Linear time-varying
MPC	Model Predictive Control
NED	North-East-Down
OSC	Outer Semicontinuous
PI	Proportional-Integral
PID	Proportional-Integral-Derivative
QP	Quadratic Programming
TMO	Translational Motion Observer
UGAS	Uniformly Globally Asymptotically Stable
UGpAS	Uniformly Globally pre-Asymptoptic Stable
ULES	Uniformly Locally Exponentially Stable
USGES	Uniformly Semi-globally Exponentially Stable
VVR	Virtual Vertical Reference

Symbols

System states	
η	Position and attitude
ν	BODY frame velocity
ν_r	Relative BODY frame velocity
p	NED position
v	NED velocity
Kinetics	
M	Inertia matrix including hydrodynamic mass
$C(\nu)$	Rigid-body and hydrodynamic Coriolis matrix
$D(\nu)$	Damping matrix
τ	Body frame force
b	Bias force
Kinematics	
$J_k(\eta)$	6DOF transformation matrix from BODY to NED
$R(\psi)$	3DOF transformation matrix from BODY to NED
$S(a)$	Cross-product matrix operator. $S(a)b = a \times b$
Inertial Navigation	
f_{ib}^b	Specific force
ω_{ib}^b	Angular rates
f_{imu}^b	IMU acceleration measurement
ω_{imu}^b	IMU angular rate measurement
b	Sensor bias
w	Sensor noise
Control Allocation	
α	Vector of azimuth angles
$B(\alpha)$	Thrust configuration matrix
u	Vector of thrust setpoints
Hybrid Systems	
$\mathcal{H}(C, F, D, G)$	Hybrid system
C	Flow set
F	Flow map
D	Jump set
G	Jump map

Contents

List of Figures

List of Tables

Chapter 1

Introduction

The topic of this thesis is control allocation and observer design for autonomous ferries. In this section some background and motivation for increased autonomy in ferry operations is presented together with an introduction to the operation and construction of double-ended car ferries.

1.1 Background and motivation

In the recent years, there has been a significant increase in the activity related to autonomy in ships, both in academia and in the industry. The motivating factors for increased autonomy are multiple. Operational costs may be cut by reduced manning and optimized operation. Safety may be improved by limiting human errors and reducing the number of humans involved in the operation. Also, it may enable operations that are impossible or impractical with a human operator. To realize this, a lot of new work needs to be done both in the technology, regulations and integration with existing solutions.

To build confidence and social acceptance in the technology, the first uses of autonomous ships needs to be simple. Due to its relatively low mission complexity, ferries are proposed as a good candidate for piloting the transition towards increased autonomy in ships.

Several research and industry projects related to autonomous ferry operations exist already, most within double-ended car ferries. Rolls-Royce Marine (now Kongsberg Maritime) has a contract with Fjord 1 AS to deliver auto-

crossing capabilities at 18 ferry sites in Norway [33]. Kongsberg Maritime has a contract with Torghatten AS to deliver an automated crossing and docking system for the Bastø-Fosen strech [37]. Wartsila has developed an autocrossing and autodocking system for NORLED AS with succesful full-scale tests [41]. Also, the Autoferry project at NTNU is developing a small, unmanned ferry to carry passangers and bikes across the Trondheim channel [40].

(a) The Autoferry prototype milliAmpere docking at Ravnkloa in Trondheim. Photo: Kai Dragland

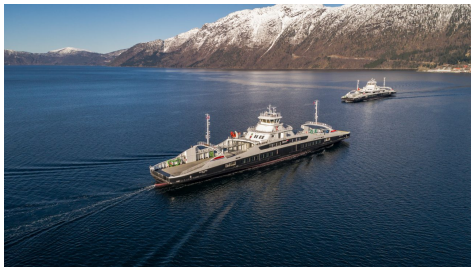

(b) The sister ships MF Gloppefjord and MF Eidsfjord crossing the Anda-Lote strech with auto-crossing system from Rolls-Royce Marine. Source: Fjord1

Figure 1.1: Examples of activity related to autonomy in ferry operations.

1.2 Operation and construction of double-ended ferries

This thesis will focus on double-ended car ferries, an introduction to their construction and the way they operate is given next.

The objective of double-ended car ferries is to connect a road separated by a short distance of water. These are particularly common in Norway, with its many narrow fjords interrupting normal traffic flow along the western coast. As of 2017, there was about 150 connections in Norway, carrying 43 million people and 21 million vehicles [31].

Double-ended car ferries have fore-aft symmetry and have gates opening at both sides to allow cars to roll on and off without having to back their way

out. Normally, they also have fore-aft symmetry in the thruster configuration, having one centered azimuth thruster in each end. See Figure 1.2.

Figure 1.2: Typical construction and thruster configuration of a double-ended car ferry. Source: Skipsrevyen

A crossing operation may be divided into several phases, or modes of operation. In this thesis, the following modes are defined for a crossing from A to B:

1. **Takeoff from A**: The ferry leaves the dock at A and accelerates to service speed.
2. **Transit A to B**: The ferry travels at a constant service speed for the majority of the crossing.
3. **Transition A to B**: As the ferry approaches the dock at B, it decelerates from service speed to low speed and positions itself for docking.
4. **Docking at B**: The ferry maneuvers at low speed until it enables contact with the dock at B.

5. **Dockside at B**: The ferry thrusts against the dock at B to keep the ferry in place while unloading and loading cars and passengers.

After finishing the on-loading at B, the same process repeats itself from B to A. A typical speed profile and route is shown in Figure 1.3, with corresponding modes of operation.

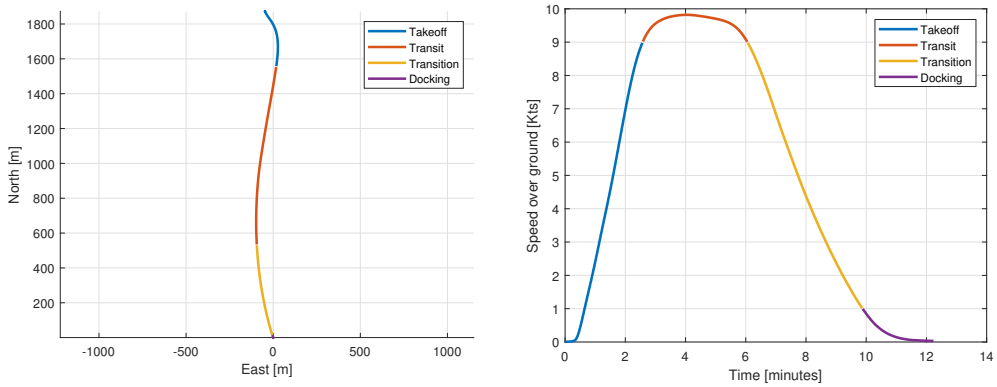

(a) Sample route

(b) Sample speed profile

Figure 1.3: A typical route and speed profile for a crossing operation.

1.3 Main contributions

The main contributions of this thesis are two research papers on topics related to control of autonomous ferries:

Paper 1: Control allocation for double-ended ferries *Submitted for publication to the 2019 Control Applications for Marine Systems, CAMS 2019.* A novel control allocation algorithm is presented for ferries with one centered azimuth thruster in each end. The allocation problem is formulated as a nonlinear optimization problem. Using the symmetry of the thruster configuration, a fast and robust solution method for the nonlinear optimization problem is proposed. The algorithm is verified through simulations and full-scale experiments.

Paper 2: A resetting observer for LTV systems with applications to dynamic positioning of marine surface vessels *To be submitted to the 2020 American Control Conference, ACC 2020.* A resetting observer for

generic linear time-varying systems is presented. If the output estimation error exceeds predefined bounds, the observer makes a jump to a more correct state estimate. The new estimate after a jump is calculated using a finite-time observer approach. The observer has important applications to dynamic positioning of marine surface vessels, as it may increase the transient performance. The observer is tested in a simulation study with an offshore supply vessel.

1.4 Organization of the thesis

This thesis is a step towards a PhD, as the presented material is within the research plan for the PhD, being an integrated MSc and PhD candidate. This thesis is therefore edited as a collection of papers with a resume in front. The resume presents relevant background theory in marine control systems and hybrid systems. This aims to ease the readability of the papers, present existing methods and to put the contributions of this thesis into a context. A simulation study is also included to show how the components developed in the papers may be used in the control system of an autonomous car ferry.

Chapter 2 gives the background in modelling and control of marine surface vessels. The control architecture is presented, and the main components are introduced. Particular emphasis is put on the control allocation and observer parts.

Chapter 3 introduces the field of hybrid systems. First an overview of the field is given, followed by a historic review. Some recent applications to marine control system are also presented. Finally, the mathematical framework used in the formulation and analysis of the resetting observer in Paper 2 is presented in-depth.

Chapter 4 presents a case study for autonomous docking of a double-ended car ferry. The ferry-site and vessel is briefly introduced, and a high-fidelity simulator for the ferry is presented. Finally, simulation results are presented and discussed.

Concluding remarks and recommendations for further work are given in Chapter 5.

Appendix A lists the numerical values for the parameters used in the case study. Appendix B shows the cost function used in the control allocation in the case study. Appendix C contains the two papers.
The recommended order of reading is to first read the preliminaries in Chapter 2 and 3, followed by the appended papers of Appendix C and finally the case study of Chapter 4 and the conclusions in Chapter 5.

Chapter 2

Mathematical modelling and control of marine vessels

This chapter presents some preliminaries in modelling and control of marine vessels, relevant for control of autonomous ferries. The control control architecture is presented, and all block are given a brief introduction. The observer and control allocation blocks are presented in greater detail, and some existing solutions are introduced to give perspective on how the contributions of this thesis distinguish themselves from these.

2.1 Modelling of marine surface vessels

2.1.1 Notation and frames of reference

This thesis adopts the notation used in [22], building on the SNAME 1950 standard notation. The reader is referred there for details on the notation and symbols.

Two important frames of reference are used in this thesis: The inertial **NED frame**, with origin at a fixed point relative to the earth surface, and axis pointing North, East and Down, and the **BODY frame**, with origin at a point fixed to the vessel and axis pointing in surge, sway and heave.

The definition of the BODY frame axis for a ship is shown in Figure 2.1.

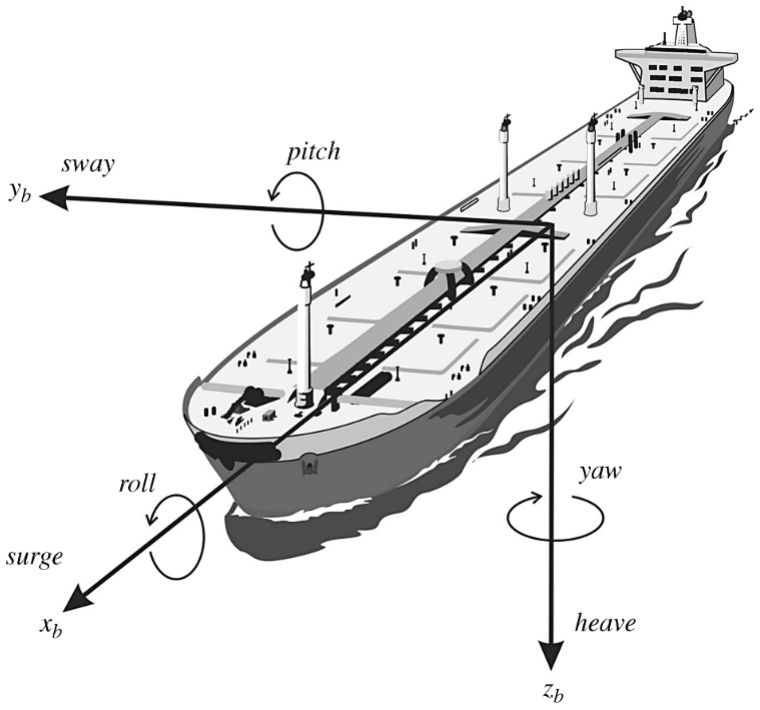

Figure 2.1: Definition of ship coordinate axis. Source: [22].

Variables in BODY frame are denoted by superscript b, and variables in NED frame are denoted by superscript n. In cases where it is not obvious, variable expressing motion of frame b relative to frame a are denoted by subscript ab.

Element i of a vector v is denoted $v_{(i)}$. The entry in row i and column j of a matrix M is denoted $M_{(i,j)}$.

2.1.2 Vessel kinematics and kinetics

The kinematic and kinetic equations of motion for a general six degree of freedom marine vessel is derived in [22], using vectorial mechanics:

$$\dot{\eta} = J_k(\eta)\nu \tag{2.1}$$

$$M\dot{\nu} + C(\nu)\nu + D(\nu)\nu + g(\eta) + g_0 = \tau + \tau_{wind} + \tau_{wave} + \tau_{curr} \tag{2.2}$$

where $\eta \in \mathbb{R}^{6\times1}$ is the position and orientation in NED frame, $\nu \in \mathbb{R}^{6\times1}$ is the linear and angular velocities in BODY frame. $J_k(\eta) \in \mathbb{R}^{6\times6}$ is a transformation matrix mapping the BODY velocities to NED velocities. $M \in \mathbb{R}^{6\times6}$ is the rigid body and added mass matrix, $C(\nu)\nu$ contains centripital and coriolis forces and moments due to (2.2) being expressed in the non-inertial BODY frame. $D(\nu)\nu$ is a damping term, and $g(\eta) + g_0$ are gravitational and hydrostatic forces and moments. The right hand side (RHS) of (2.2) represents the exiting forces, and may include thruster forces, $\tau \in \mathbb{R}^{6\times1}$, wind loads, $\tau_{wind} \in \mathbb{R}^{6\times1}$, wave loads, $\tau_{wave} \in \mathbb{R}^{6\times1}$ and current forces, $\tau_{curr} \in \mathbb{R}^{6\times1}$ Current forces may also be added by using the relative velocity through the water, ν_r in place of ν. This requires the assumption of constant, irrotational currents and a special parametrization of $C(\nu)\nu$. See [22] for details. This model does not include lift forces, and is therefore not applicable for very high speeds [9].

2.1.3 Low speed vessel model

The general six degree of freedom model of (2.1)-(2.2) may be reduced to a three degree of freedom control plant model describing the horizontal motion (surge, sway and yaw):

$$\dot{\eta} = R(\psi)\nu \tag{2.3}$$

$$M\dot{\nu} + D\nu = R^T(\psi)b + \tau + \tau_{wind} + \tau_{wave}. \tag{2.4}$$

$$\dot{b} = 0 \tag{2.5}$$

This is a valid model reduction under the assumption of low speed. Then, the coriolis and centripetal forces are negligible and linear viscous damping dominates. The current forces and unmodelled dynamics from (2.2) are modelled as a slowly varying bias term $b \in \mathbb{R}^{3\times1}$. $R(\psi) \in \mathbb{R}^{3\times3}$ contains the surge, sway and yaw terms of $J_k(\eta)$ with the assumption of zero roll and pitch.

This model is used in DP observer and control design.

2.1.4 Autopilot model

By again considering the horizontal degrees of freedom in (2.1)-(2.2), linearizing the kinetics about a service speed and supressing the second order dynamics, the first order autopilot model of Nomoto is obtained:

$$T\ddot{\psi} + \psi = K\delta \tag{2.6}$$

where ψ is the heading, T is a time constant determined by the inertial and damping properties of the ship, δ is the rudder angle and K is the rudder constant.

This model is used in transit observer and control design.

2.2 Control architecture

A typical control architecture for a marine surface vessel is shown in Figure 2.2. An autonomous ferry will also need additional high-level control components such as situational awareness, path planning and collision avoidance. However, since high-level control is not relevant for this thesis, this is not included here.

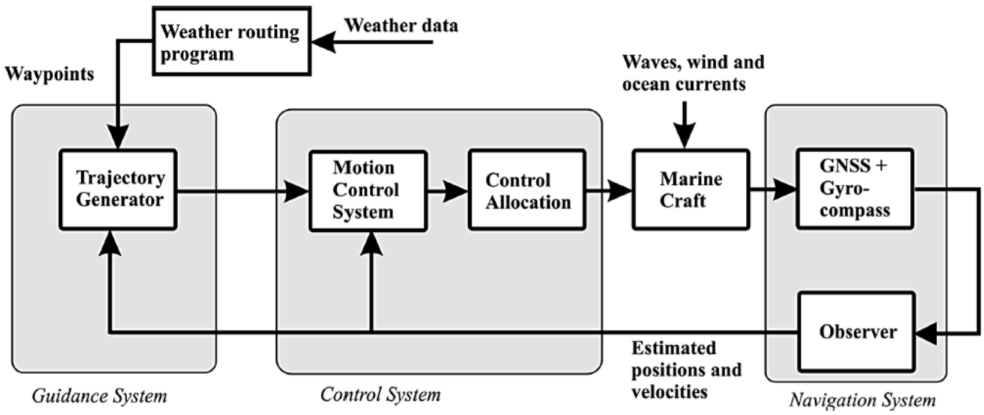

Figure 2.2: Control architecture for a marine surface vessel. Source: [22]

2.3 Motion control

Two classes of motion control methods are presented next. Dynamic positioning is relevant for the docking mode of operation, whereas autopilot is used during transit the transit mode of operation.

2.3.1 Dynamic positioning

The control objective in dynamic positioning is station keeping or low speed maneuvering. Normally, only the horizontal degrees of freedom are controlled, but in vessels with small waterplane area, roll and pitch damping may also be included [35].

A horizontal plane control law may be synthesized from the control plant model of (2.3)-(2.4). For station keeping applications with small deviations about a fixed desired heading, ψ_d, a linear PID control law may be used [35]:

$$\tilde{\eta}_p = R^T(\psi_d)(\eta - \eta_d) \tag{2.7}$$

$$\tilde{\nu} = \nu - \nu_d \tag{2.8}$$

$$\dot{\xi} = \tilde{\eta}_p \tag{2.9}$$

$$\tau = -K_p\tilde{\eta}_p - K_d\tilde{\nu} - K_i\xi \tag{2.10}$$

where script d denotes reference signals, and K_p, K_d, $K_i \in \mathbb{R}^{3\times3}$ are the proportinal, derivative and integral gain matrices, respectively. For (2.7)-(2.10), linear control synthesis methods such as LQR or pole-placement can be used. Note that this control law is based on a linearization of (2.3)-(2.4) about the desired heading.

For low speed maneuvering applications, the nonlinear PID control law of [22], with reference feedforward, is more appropriate:

$$\begin{aligned}\tau = &-R^T(\psi)K_p(\eta - \eta_d) - K_d(\nu - \nu_d) \\ &- R^T(\psi)K_i\int(\eta - \eta_d)dt + Ma_d + D\nu_d\end{aligned} \tag{2.11}$$

$a_d \in \mathbb{R}^{3\times 1}$ is the acceleration reference in the BODY frame. Note that the actual heading angle, ψ is used in the rotation matrices, instead of the constant desired heading as seen in the linear PID control law. Note also that the integrator is expressed in NED coordinates. This is rationalized by the fact that the integral term counteracts slowly varying loads such as current and wind, which are usually changes less in the NED frame than the BODY frame.

2.3.2 Autopilot

The control objective of an autopilot system is to track a desired heading at constant forward speed, u_d. Autopilot systems differ in complexity, from simple constant course keeping controllers to path following systems tracking heading references from a guidance system.

A simple PID autopilot control law based on the control plant model of (2.6) can be used:

$$\tau_N = -K_p(\psi - \psi_d) - K_d(r - \dot{\psi_d}) - K_i \int (\psi - \psi_d)dt \tag{2.12}$$

Knowing the Nomoto time constant in (2.6) and the rigid body and added mass in yaw, pole placement may be used in the control design. Note that under presence of current, the heading and course will differ. Methods to handle this include sideslip estimation and adding integral action to the guidance law. See [22] for details.

In an autonomous autopilot system, a speed controller is also necessary to maintain a constant forward speed. Since there is only one integrator between thruster force and speed, a PI controller is appropriate:

$$\tau_X = -K_p(u - u_d) - K_i \int (u - u_d)dt \tag{2.13}$$

Here, u_d is the speed reference.

2.4 Guidance

The purpose of the guidance system is to provide the motion controllers with smooth references. In this section, two common guidance laws are presented. The first is relevant for the crossing mode of operation and the latter is relevant for the docking mode of operation.

2.4.1 Line-of-sight

In *path following*, the control objective is to follow a predefined path without any temporal restrictions along the path [22]. In the case of a path defined by line-segments between waypoints, this may be solved by the *Line-of-sight* (LOS) guidance law, as shown in Figure 2.3

The idea in line-of-sight guidance is to steer towards a point which is a fixed distance, Δ, along the path in front of the ship. This is called the *lookahead* distance. Given a linear path, $\mathcal{P}$ from point P_0 to P_1, a coordinate frame is defined with the x-axis running along the path, and the y-axis perpendicular to the path. The origin of this frame is at P_0.

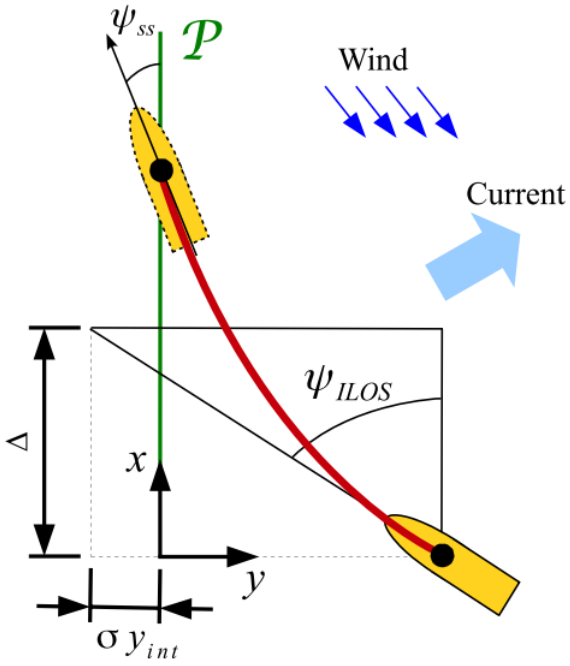

Figure 2.3: ILOS guidance for surface vessels. Source: [30]

y is called the *cross-track error*, and the control objective in path following of linear paths may thus be expressed as:

$$\lim_{t\to\infty} y(t) = 0 \tag{2.14}$$

In presence of disturbances such as currents and wind, the vessel may need to crab at a steady state heading angle, ψ_{ss} to track the path with zero steady state offset. To accommodate this, integral effect is introduced. The resulting guidance law is known as *Integral Line-of-sight* (ILOS).

The ILOS guidance law is given by [30]:

$$\psi_{ILOS} = -\arctan(\frac{y + \sigma y_{int}}{\Delta}) \tag{2.15}$$

$$\dot{y}_{int} = \frac{\Delta y}{(y + \sigma y_{int})^2 + \Delta^2} \tag{2.16}$$

where σ is an integral gain.

Caharija et al. shows that the equillibrium point for a simplified vessel model with the ILOS guidance law is Uniformly Globally Asymptotically Stable (UGAS) ans Uniformly Locally Exponentially Stable (ULES) under certain assumptions. See [30] for details.

2.4.2 Reference filter

For DP applications, a guidance law is often introduced to provide smooth trajectories during setpoint changes. A common approach is to use a third order transfer function from setpoint to reference [22]:

$$\eta_d^{(3)} + (2\Gamma + I_{3\times3})\Omega\ddot{\eta}_d + (2\Gamma + I_{3\times3})\Omega^2\dot{\eta}_d + \Omega^3\eta_d = \Omega^3 r^n \tag{2.17}$$

where $\eta_d \in \mathbb{R}^{3\times1}$ is the position reference, $r^n \in \mathbb{R}^{3\times1}$ is the setpoint, $\Gamma \in \mathbb{R}^{3\times3}$ is a diagonal matrix of filter damping rations and $\Omega \in \mathbb{R}^{3\times3}$ is a diagonal matrix of filter natural frequencies.

To ensure feasible references to follow for all ranges of setpoints, saturation elements should be added for velocity and acceleration. A block diagram of the reference filter in (2.17) with saturation elements is shown in Figure 2.4.

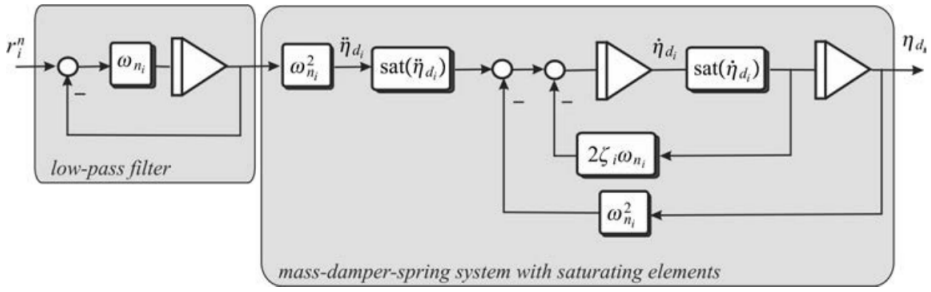

Figure 2.4: Third order reference filter with saturation on velocity and acceleration. Source: [22]

Note that this is an *open-loop guidance law*. This is, its output does not depend on the position of the ship. Also, having the reference be the solution of a differential equation, as in (2.17), may not always yield the desired

behaviour. Fernandez proposes an alternative solution in [27], by dividing a setpoint change into 4 phases, and stitching together smooth trajectory.

2.5 Observer

The observer is a vital part of an autonomous navigation system. Its purpose is to do filtering of measurements to remove noise and wave frequency components, and also to estimate unmeasured states. For marine surface vessels, velocity is usually not measured, and thus needs to be estimated. Measurements from a Global Navigation Satellite System (GNSS) of speed over ground and course over ground are available, but the measurement quality is often poor at low speeds. This section presents different observers from the two main classes of existing methods; Model based observer and inertial navigation.

2.5.1 Model based observers

Model based observers have been used successfully in DP systems for decades. Examples include the Kalman Filter[2], Extended Kalman Filter[35], and Passive Nonlinear Observer [11]. They all have in common that disturbances and modelling errors are handled by a slowly varying bias term. Often, this renders them too slow to capture transient behaviour.

When designing a model based observer, a specific model must be chosen. If the assumptions of this model is not met, the performance may be poor. Finding a unified control plant model for low-speed and high-speed regimes is very difficult. Using a single model based observer for all operational modes in a ferry operation is thus not feasible. An option is to use hybrid switching approach, as in [18] and [20].

The state-of-the-art control plant model used in observer design for DP is given by [35]:

$$\dot{\xi} = A_w \xi \tag{2.18a}$$

$$\dot{\eta} = R(\psi)\nu \tag{2.18b}$$

$$\dot{b} = -T_b^{-1} b \tag{2.18c}$$

$$M\dot{\nu} + D\nu = \tau + R^\top(\psi)b \tag{2.18d}$$

$$y = \eta + C_w\xi \tag{2.18e}$$

where $\xi \in \mathbb{R}^6$ are the states of a second-order harmonic oscillator, modelling the wave frequency motion of the vessel, $\eta \in \mathbb{R}^3$ is the position and heading, $\nu \in \mathbb{R}^3$ is the body frame velocity and turn rate, $b \in \mathbb{R}^3$ is a bias term and $\tau \in \mathbb{R}^3$ is the body frame thruster forces. $A_w \in \mathbb{R}^{6\times6}$ is the state space matrix for a second order harmonic oscillator, $R(\psi) \in \mathbb{R}^{3\times3}$ is a three degree of freedom rotation matrix, $T_b \in \mathbb{R}^{3\times3}$ is a diagonal matrix of bias time constants, $M \in \mathbb{R}^{3\times3}$ is the mass matrix, including added mass, and $D \in \mathbb{R}^{3\times3}$ is the linear damping matrix.

Using this model, a Luenberger-like observer can be designed:

$$\dot{\hat{\xi}} = A_w\hat{\xi} + K_1\tilde{y} \tag{2.19a}$$

$$\dot{\hat{\eta}} = R(\hat{\psi})\hat{\nu} + K_2\tilde{y} \tag{2.19b}$$

$$\dot{\hat{b}} = -T_b^{-1}\hat{b} + K_3\tilde{y} \tag{2.19c}$$

$$M\dot{\hat{\nu}} + D\hat{\nu} = \tau + R^\top(\hat{\psi})\hat{b} + R(\hat{\psi})^\top K_4\tilde{y} \tag{2.19d}$$

$$\hat{y} = \hat{\eta} + C_w\hat{\xi} \tag{2.19e}$$

The injection gain matrices $K_1 \in \mathbb{R}^{3\times6}$, $K_2 \in \mathbb{R}^{3\times3}$, $K_3 \in \mathbb{R}^{3\times3}$ and $K_4 \in \mathbb{R}^{3\times3}$ can be calculated using an Extended Kalman Filter [35] or using a passivity approach [11].

2.5.2 Inertial navigation

By extending the sensor suite to include an *Inertial Measurement Unit* (IMU), it is possible to design observers that address the issues raised by model based observers in Section 2.5.1. Inertial Measurement Units include accelerometers and rate gyros. These signals can be used in place of a kinetic model in an observer, and thus yield a model free approach. Observers based on inertial navigation typically also have better transient behaviour [34].

An IMU measures *specific force*, $f_{ib}^b \in \mathbb{R}^{3\times1}$ and angular rates $\omega_{ib}^b \in \mathbb{R}^{3\times1}$. f_{ib}^b is the acceleration of the IMU casing relative to an inertial frame, i, plus the gravitational acceleration. It is decomposed in body frame coordinates. Both

sensor measurements, $f^b_{imu} \in \mathbb{R}^{3\times1}$ and $\omega^b_{imu} \in \mathbb{R}^{3\times1}$, are usually corrupted by sensor noise and sensor bias. The following sensor model is therefore used [29]:

$$\omega^b_{imu} = \omega^b_{ib} + b^b_{ars} + w^b_{ars} \tag{2.20}$$

$$f^b_{imu} = f^b_{ib} + b^b_{acc} + w^b_{acc} \tag{2.21}$$

where $\omega^b_{ib} \in \mathbb{R}^{3\times1}$ and $f^b_{ib} \in \mathbb{R}^{3\times1}$ are the true values, $b^b_{ars} \in \mathbb{R}^{3\times1}$ and $b^b_{acc} \in \mathbb{R}^{3\times1}$ are bias terms and $w^b_{ars} \in \mathbb{R}^{3\times1}$ and $w^b_{acc} \in \mathbb{R}^{3\times1}$ are noise terms.

The bias term in the rate gyros may be substantial, and have poor in-run stability. That is, it can change while operating, and can therefore not be cancelled by pre-run calibration. Hence, it must be estimated and compensated for online. The bias term in the accelerometers typically have better in-run stability, and they are difficult to estimate online. In fact, for a combined attitude and position observer, observability is lost when including an unknown accelerometer bias. The standard practice is therefore to do pre-run calibration to compensate for this [22].

The kinematics on an inertial navigation system are governed by the *Strapdown Inertial Equations*. Under the assumption of NED being inertial, these are given by [29]:

$$\dot{p}^n_{nb} = v^n_{nb} \tag{2.22}$$

$$\dot{v}^n_{nb} = R^n_b f^b_{ib} + g^n_b \tag{2.23}$$

$$\dot{R}^n_b = R^n_b S(\omega^b_{nb}) \tag{2.24}$$

Here, $p \in \mathbb{R}^{3\times1}$ is linear position, $v \in \mathbb{R}^{3\times1}$ is linear velocity and $g \in \mathbb{R}^{3\times1}$ is the gravitational acceleration. $S \in \mathbb{R}^{3\times3}$ is a skew symmetric matrix, such that $S(a)b = a \times b$. See [22] for details.

When using INS based observers for marine vessels, it is required by class that they are backed by model based observers for redundancy in case of a sensor failure. Model based observers also have the advantage of not being linked to a physical device. In an operational setting, this is appreciated

since the user does not need to worry about hardware specific challenges, such as alignment errors, calibration, sensor integrity etc. Because of this, model based observers are still the industry standard.

GNSS aiding

The linear position and velocity and the attitude may be estimated by integrating the strapdown inertial equations. This gives very high accuracy at short time horizons. However, due to sensor bias, misalignment errors etc. the estimates will drift over time. To resolve this, the observer needs to be corrected by an external position and attitude reference.

Several observers based on variations of Extended Kalman Filters (EKF) have be suggested over the years, with good results [29]. However, a caveat with the EKF is the lack of global stability results. Because of this, researchers have investigated nonlinear observers for GNSS/INS integration, including Salcudean (1991) [4], Vik et al. (2001) [13] and Mahony et al. (2008) [19].

Building on this, Grip et al. proposed a nonlinear observer for GNSS aided inertial navigation in 2015 [28]. Instead of estimating the attitude vector, the rotation matrix is estimated directly:

$$\dot{\hat{R}} = \hat{R}S(\omega^b_{imu} - \hat{b}^b_{ars}) + \sigma K_P \hat{J} \tag{2.25}$$

$$\dot{\hat{b}}^b_{ars} = Proj(\hat{b}^b_{ars}, -k_I vex(\mathbb{P}_a(\hat{R}^T_s K_P \hat{J}))) \tag{2.26}$$

Again, S is a skew symmetric matrix representing the cross product operator in matrix form. The operator $\mathbb{P}_a(X)$ denotes the skew symmetric part of a matrix X: $\mathbb{P}_a(X) = \frac{1}{2}(X - X^T)$. The function $vex(X)$ is defined such that $S(vex(X)) = X$ and $vex(S(x)) = x$ for all skew-symmetric matrix arguments. $Proj(\cdot, \cdot)$ is a special case of the Parameter Projection function, which makes sure that the gyro bias estimate stays bounded. $\hat{J} \in \mathbb{R}^{3\times3}$ is a stabilizing injection term for attitude measurements, which may take several forms. σ, K_P and k_I are tunable constants. See [28] for details.

The author proposed a novel stabilization injection term, $\hat{J}$, for this attitude observer in [36]. Results from high-fidelity simulation indicated improved

roll and pitch estimation compared to existing methods.

The translational motion observer (TMO) uses the estimated rotation matrix from (2.25) and (2.26), integrates acceleration measurements and corrects by injection of position and velocity measurements:

$$\dot{\hat{p}}^n = \hat{v}^n + K_{pp}(p^n - \hat{p}^n) + K_{pv}(v^n - C_v\hat{v}^n) \tag{2.27}$$

$$\dot{\hat{v}}^n = \hat{f}^n + g^n + K_{vp}(p^n - \hat{p}^n) + K_{vv}(v^n - C_v\hat{v}^n) \tag{2.28}$$

$$\dot{\xi} = -\sigma K_P \hat{J} f_{imu} + K_{\xi p}(p^n - \hat{p}^n) + K_{\xi v}(v^n - C_v\hat{v}^n) \tag{2.29}$$

$$\hat{f}^n = \hat{R} f_{imu} + \xi \tag{2.30}$$

Where K_{pp}, K_{pv}, K_{vp}, K_{vv}, $K_{\xi p}$ and $K_{\xi v}$ are observer gains, and C_v is a selection matrix extracting the degrees of freedom for which we have measurements from v^n. In [28] it is shown that the origin of the error dynamics for the combined GNSS/INS observer is Globally Exponentially Stable (GES), under reasonable assumptions.

Bryne et al. introduced the Virtual Vertical Reference (VVR) for GNSS aided INS in vessels operating at the ocean surface [26]. This work was motivated by the poor vertical measurements provided by GNSS systems. The main idea is to use the fact that the vessel oscillates about zero vertical position, and the average vertical position is thus zero. This is equivalent to saying that the integral of vertical position over time approaches zero as time goes to infinity. By augmenting the observer with a state for the integral of the vertical position estimate, this can be injected into the position observer and keep the vertical position estimate from drifting. Bryne et al. went on to prove that the origin of the error dynamics of a translational motion observer for surface vessels with VVR and the attitude observer of Grip et al. (2013) [24] is Uniformly Semi-globally Exponentially Stable (USGES). The attitude observer of Grip et. at (2013) is closely related to that of (2.25)-(2.26), but uses quaternion estimation instead of the Euler angel rotation matrix. See [26] for details.

In 2018, Brodtkorb et al. used the attitude observer of (2.25)-(2.26) together with the translational motion observer of Bryne et al. (2015) and states that the combined system is GES. See [34] for details.

2.6 Control allocation

This section provides an overview of the control allocation problem and the two most common classes of methods. For an in-depth review of control allocation methods, the reader is referred to [17] and [25]. A more recent approach by Skjong and Pedersen (2017) formulates the thrust allocation problem as an MPC problem, and thus finds an optimal sequence of allocations within a time horizon [32].

2.6.1 The control allocation problem

Control allocation is the problem of allocating the desired control action for a vehicle to its actuators. For marine vessels this is often referred to as *thrust allocation*.

For marine vessels with the horizontal plane as its working space, the input to the thrust allocation module is the desired body frame control action $\tau = [X, Y, N]^T$. The output from the thrust allocation is the setpoints to the propulsors. This can be in form of e.g. propeller speed, propeller pitch, azimuth angle or rudder angle, depending on the type of the propulsor.

The mapping from actuator setpoints to body frame control action can be formulated as

$$\tau = B(\alpha)u \tag{2.31}$$

where α is a vector of unknown actuator angles and u is an unknown vector of thrust setpoints. The matrix B is called the *thrust configuration matrix*. The system of (2.31) is in many cases under-determined, that is, there are infinitely many solution. This gives the thrust allocation algorithm freedom to choose one that is optimal in some sense.

2.6.2 Pseudo inverse solution

In the case where the thrust configuration matrix, B, does not depend on α, a widely used method is the pseudo inverse (Moore-Penrose inverse). The pseudo inverse is a generalisation of an inverse matrix for non-square matrices. In relation to solving linear systems of equations, it has the property that is provides the minimum 2-norm solution, that is, it minimizes the squared sum of thrusts. The pseudo inverse, $B^\dagger$, of a matrix, B can be calculated explicitly from

$$B^\dagger = (B^T B)^{-1} B^T \tag{2.32}$$

The thrust setpoints can then be calculated as

$$u = B^\dagger \tau \tag{2.33}$$

The advantages of the pseudo inverse method is simplicity and low computational cost. The pseudo inverse of the thrust configuration matrix can be pre-computed once, and solving the thrust allocation problem is then reduced to a matrix-vector multiplication. One weakness of the method is that it only optimizes for thrust norm, whereas other objectives may be more important in some cases. Also, it can not be applied when the thrust configuration matrix depends on the thruster angles. The main limitation is, however, that constraints other than the thrust configuration constraint of (2.31) can not be added.

2.6.3 Quadratic programming solution

In the case of azimuthing thrusters, a widely used approach is to formulate the thrust allocation problem as a quadratic programming (QP) problem. Different objective functions are possible, but it is common to minimize power consumption and azimuth angle change. A QP problem must have a convex, quadratic function objective function, and linear constraints. Both the power consumption and the thrust configuration constraint are, in general, nonlinear and must thus be linearized.

A QP problem which minimizes power consumption and angle change, and constrains the change of angle, maximum and maximum thrust can be formulated as [17]:

$$\min_{\Delta f, \Delta\alpha, s} J = (f_0 + \Delta f)^T P (f_0 + \Delta f) + s^T Q s + \Delta\alpha^T \Omega \Delta\alpha \tag{2.34}$$

subject to

$$s + B(\alpha_0)\Delta f + \frac{\partial}{\partial \alpha}(B(\alpha) f)|_{\alpha_0, f_0} \Delta\alpha = \tau - B(\alpha_0) f_0 \tag{2.35a}$$

$$f_{min} - f_0 \leq \Delta f \leq f_{max} - f_0 \tag{2.35b}$$

$$\alpha_{min} - \alpha_0 \leq \Delta\alpha \leq \alpha_{max} - \alpha_0 \tag{2.35c}$$

$$\Delta\alpha_{min} \leq \Delta\alpha \leq \Delta\alpha_{max} \tag{2.35d}$$

Here, f_0 and α_0 are the thrusts and angles from the last time step, and Δf and $\Delta\alpha$ are the change from last to current time step. Furthermore, s is a vector of slack variables, and P, Q, Ω are weight matrices.
This method has the advantage over the Pseudo inverse method in that is can optimize for a more general objective, and constraints can be added. The challanges with this method is increased computational cost, and the fact that it is a linearization of the actual problem. Since the optimization problem is linearized about the last solution, the solver can only optimize locally about this point and thus lacks a global perspective.

Chapter 3

Hybrid systems and control

Hybrid dynamical systems are systems with both continuous and discrete dynamics. Many phenomena may be modelled naturally as hybrid dynamical systems, and hybrid approaches opens up for many new possibilities for control of dynamical systems. Because of this, a lot of work has been done in the field of hybrid systems and control over the past decades.

This chapter reviews the literature and history of hybrid systems and control and then gives an in-depth presentation of a mathematical framework for modelling and analysis of hybrid dynamical systems. This framework is used in the formulation and analysis of the resetting observer in Paper 2.

3.1 Overview

One can argue that hybrid control systems have been in use for a long time, for example with the introduction of relay switch circuits, introduced in the 1830's [38]. The earliest academic work related explicitly to hybrid systems dates back to the work of Witsenhausen at MIT in 1966 [1]. Since then, many quite different approaches has been taken to the modelling and analysis of hybrid systems. These may be coarsly divided into four paradigms [8]:

- **Aggregation**: The continuous dynamics are suppressed so that the hybrid system is approximated by a finite automaton or a discrete-event dynamical system.
- **Continuation**: Complmentary to aggreation, the discrete dynamics

are supressed to yield a system of differential equations.

- **Automata approach**: View the hybrid system as a network of interacting automata based on an input-output language behaviour.
- **Systems approach**: View the hybrid system as interacting dynamical systems, usually described by differential and difference equations.

The different approaches highlight different aspects of hybrid systems, and are suitable for analyzing different phenomena. There is also a trade-off between the expressiveness of a model and the properties you can prove for the model. The automata approach has been most used by the computer science community, whereas the systems approach has been most used by the control engineering community.

The discrete phenomena related to hybrid systems may be classified into four cases [8], and different approaches to the modelling are only suited for analyzing a subset set of these:

- **Autonomous switching**: The vector field describing the continuous dynamics undergoes discontinuous changes based on the conditions on the continuous states.
- **Autonomous jumps**: The continuous state undergoes discontinuous jumps based on the conditions on the continuous states.
- **Controlled switching**: The vector field describing the continuous dynamics changes discontinuously in response to a control input.
- **Controlled jumps**: The continuous state changes discontinuously in response to a control input.

The main contributions to the theory of hybrid systems originate from two research communities. Foremost, the control theory community, for which the use of hybrid systems are many. In particular, switched control systems are studied extensively. The computer science community has also made significant contributions, often with applications to software verification.

3.2 Hybrid system models

Several models have been proposed for hybrid systems. In the following, the most important ones are presented briefly in order of publication date. For a more in-depth review, the reader is referred to [8].

As mentioned, the first work related directly to hybrid systems was due to **Witsenhausen** in 1966 [1]. He proposed a model for describing autonomous switching. The dynamics of this system is described by the differential equation

$$\dot{x} = f(q(t), x(t), u(t)) \tag{3.1}$$

where $x \in \mathbb{R}^n$ is the continuous state, $q \in \mathbb{Z}$ is the discrete state and $u \in \mathbb{R}^m$ is the continuous input.
The coupling discrete dynamics are governed by the continuous state. If the discrete state $q = i$ and the continuous state enters the set $M_{i,j}$, the discrete state transitions from i to j. Under reasonable topological assumptions on $M_{i,j}$ and certain smoothness assumptions on $f(q, \cdot, \cdot)$ Witsenhausen defined the solution for this type of system, and proved the existance and uniqueness of these. He continued to give some optimal control results.

Building on the results of Witsenhausen, **Tavernini** introduced the *differential automata* in 1987 [3]. For this he proved that the initial value problem has a unique solution with finitely many switching points. The focus of his work was the analysis of numerical simulations of the solutions to differential automata.

In 1993 **Back, Guckenheimer and Myers** introduced a generalization of the Tavernini model [5]. Most notably, the model allows jumps in continuous states. The model also has a number of sets X_q for the continuous state, associated with the vector field f_q. The sets X_q are not assumed disjoint, and uniqueness can thus not be guaranteed for the solutions.

Also in 1993, **Nerode and Kohn** introduced a quite different hybrid systems model building on automata theory [7]. As illustrated in Figure 3.1, the model consists of three components:

1. A continuous time plant

2. A digital automaton

3. An interface

The interface consists of an analog-to-digital map, mapping the continuous plant state to symbols input to the digital automaton, and digital-to-analog map converting symbols from the digital automaton to continuous time inputs to the plant.

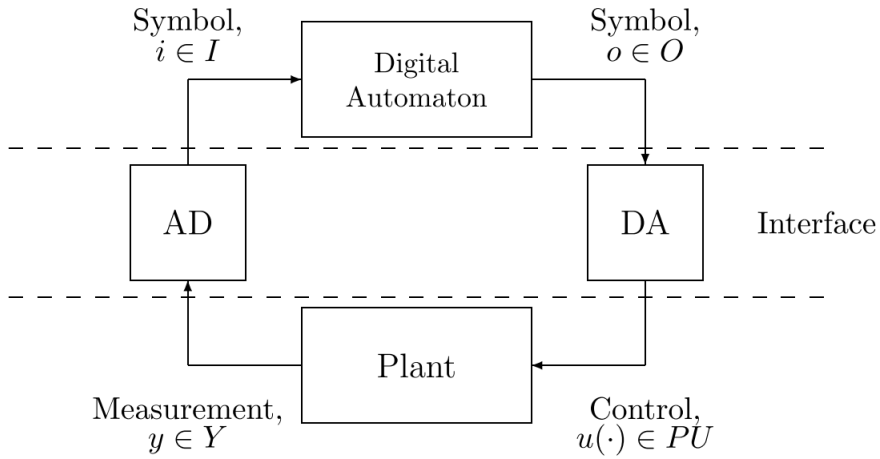

Figure 3.1: Hybrid system model of Nerode and Kohn. Figure from [8].

The same year, **Antsaklis, Stiver and Lemmon** considered discrete-event dynamical systems, which are closely related to the model of Narode and Kohn [6]. The interface between the discrete controller and the continuous plant is given particular attention. The digital-to-analog (DA) mapping, here called *actuating function*, is implemented as a piecewise constant plant input. The analog-to-digital (AD) mapping (here called *generating function*) is implemented by partitioning the state space by hyper-surfaces, and issuing symbols to the discrete controller when the continuous state crosses these.

More recently (2004) **Goebel, Hespanha, Teel, Chaohong and Sanfelice** introduced a model based on a *constrained differential inclusion* and a *constrained difference inclusion*. The notion of a generalized solution was introduced, and in the following years many of the stability results from continuous-time nonlinear systems (from e.g [15]) were proved for their hybrid system model. Because of the expressive power of this model, and the

fact that it builds on concepts that are familiar to most control engineers, this model will used in this thesis. The model is presented in detail in Section 3.4.
This model was recently extended to consider *stochastic hybrid dynamical systems*, which is still an active area of research.

3.3 Marine hybrid control systems

The predominant application of hybrid control in motion control systems is to switch between stabilizing controllers. An example is switching between a high-performance/low-robustness controller when close to the reference and a low-performance/high-robustness controller when further away. This is called *supervisory switching control*, and is treated in detail by Hespanha et al. in [12], [14] and [16]. This is not a trivial problem, because interestingly, switching between stabilizing controllers may yield an unstable hybrid system. Using the results of Hespanha et al., supervisory switching control has been successfully applied to control of aircraft and land-based vehicles.

The results of Hespanha et al. have also been used by Nguyen, Sørensen and Quek to design supervisory switching controllers for marine surface vessels. The architecture of this control system is shown in Figure 3.2. A bank of candidate controllers and candidate observers are run in parallel. A switching signal is calculated based on which observer is closest to the measured output. This was applied to switch from calm to extreme seas in 2007 [18], and from station keeping to transit in 2008 [20].

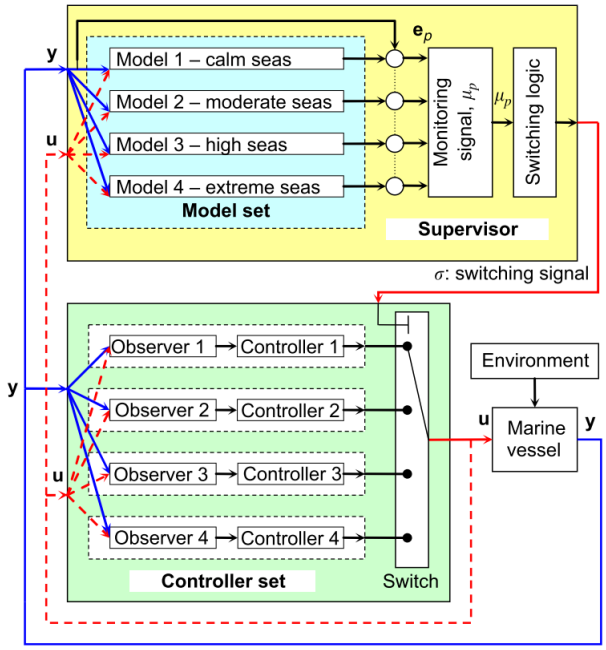

Figure 3.2: Hybrid control system architecture used by Nguyen et al. Figure from [18]

In 2016, Tutturen and Skjetne used the hybrid framework of Teel et al. [23] to design a hybrid controller to switch between agressive/non-agressive integral action for dynamically positioned vessels.

In 2018, Brodtkorb et al. designed a hybrid observer for marine vessels in DP, also using the framework of Teel et al. [34]. Here, the a passive nonlinear observer of Fossen and Stand [11] was used in steady state, and the signal based observer of Grip et al. [28], utilizing acceleration measurements, was used during transient behaviour.

3.4 A mathematical framework for hybrid dynamical systems

In Section 3.2, several mathematical frameworks for hybrid systems were presented. In this section, the framework of Goebel et al. is presented in greater

detail. This framework is very general, and thus has great expressive power. Also, it extends well known concepts from nonlinear systems theory to hybrid dynamical systems. This makes it familiar for people with a control engineering background, and also simplifies the development of stability proofs, as existing stability results for continuous components may be adopted.

This section aims to provide the reader with a minimum of background theory to understand the formulation and analysis of the resetting observer in Paper 2. The reader is referred to [23] for details. This section uses some notation and definitions from *set-valued analysis*. These concepts are briefly explained here, but the reader is referred to [10] for details.

3.4.1 The hybrid system model

In this framework, a hybrid dynamical system, $\mathcal{H} = (C, F, D, G)$, is modelled as a *constrained differential inclusion* and a *constrained difference inclusion*:

$$x \in C \quad \dot{x} \in F(x) \tag{3.2a}$$

$$x \in D \quad x^+ \in G(x) \tag{3.2b}$$

When x is in the set C, it *flows* according to the *set-valued mapping* $\dot{x} = f(x)$ for some $f \in F$. When x is in the set D, it *jumps* according to set-valued mapping $x^+ = g(x)$ for some $g \in G$. x^+ denotes the value of x after the jump.

3.4.2 The solution concept

Goebel et al. continues to give a precise definition of the solutions to $\mathcal{H} = (C, F, D, G)$. To arrive at this, two other definitions are needed first. The first is the notion of a *hybrid time domain*.

Definition 3.4.1. *Hybrid time domain ([23] Def. 2.3)*
A subset $E \subset \mathbb{R}_{\geq 0} \times \mathbb{N}$ is a compact hybrid time domain if

$$E = \bigcup_{j=0}^{J-1} ([t_j, t_{j+1}], j)$$

for some finite sequence of times $0 = t_0 \leq t_1 \leq t_2 ... \leq t_J$. *It is a hybrid time domain if for all* $(T, J) \in E$, $E \cap ([0, T] \times \{0, 1, ..., J\})$ *is a compact hybrid time domain.*

where $\cup$ is the set union, $\cap$ is the set intersection and $\times$ is the cartesian product.

Next, the notion of *hybrid arcs* is defined.

Definition 3.4.2. *Hybrid arc ([23] Def. 2.4)*
A function $\phi : E \mapsto \mathbb{R}^n$ *is a hybrid arc if* E *is a hybrid time domain and if for each* $j \in \mathbb{N}$, *the function* $t \mapsto \phi(t, j)$ *is locally absolutely continuous on the interval* $I^j := \{t : (t, j) \in E\}$.

A function is *locally absolutely continuous* if the derivative is continuous for almost all times, and the function can be recovered by integrating the derivative.

Finally, the notion of a solution to $\mathcal{H} = (C, F, D, G)$ can be defined.

Definition 3.4.3. *Solution to a hybrid system ([23] Def 2.6)*
A hybrid arc ϕ *is a solution to a hybrid system* $\mathcal{H} = (C, F, D, G)$ *if* $\phi(0, 0) \in \bar{C} \cup D$, *and*

(i) for all $j \in \mathbb{N}$ *such that* $I^j := \{t : (t, j) \in dom(\phi)\}$ *has a nonempty interior*

$$\phi(t, j) \in C \quad for\ all \quad t \in int(I^j)$$

$$\dot{\phi}(t, j) \in F(\phi(t, j)) \quad for\ almost\ all \quad t \in I^j$$

(ii) for all $t, j \in dom(\phi)$ *such that* $(t, j + 1) \in dom(\phi)$

$$\phi(t, j) \in D$$

$$\phi(t, j + 1) \in G(\phi(t, j))$$

where $\bar{C}$ is the closure of the set C, $dom(\phi)$ is the domain of ϕ and $int(I^j)$ is the interior of the set I^j.

3.4.3 Stability and robustness results

Although it is still an active area of research, there exists an extensive toolbox of analysis results for hybrid systems of the form 3.2. A special class of hybrid systems are *well-posed hybrid systems*. A system $\mathcal{H} = (C, F, D, G)$ is well-posed if it satisfies the *hybrid basic assumptions*:

Assumption 3.4.1. *Hybrid basic assumptions ([23], Assumption 6.5)*

(i) *C and D are closed subsets of $\mathbb{R}^n$*

(ii) *$F : \mathbb{R}^n \rightrightarrows \mathbb{R}^n$ is outer semicontinuous and locally bounded relative to C, $C \subset dom(F)$, and $F(x)$ is a convex set for every $x \in C$.*

(iii) *$G : \mathbb{R}^n \rightrightarrows \mathbb{R}^n$ is outer semicontinuous and locally bounded relative to D, and $D \subset dom(G)$.*

A set-valued mapping $M : \mathbb{R}^n \rightrightarrows \mathbb{R}^n$ is *outer semicontinuous* (OSC) at x if for each sequence (x_i, y_i) with $y_i \in M(x_i) \quad \forall i$ which converges to (x, y), then $y \in M(x)$. M is *locally bounded* (LB) if for each r there exists an R such that $M(r\mathbb{B}) \subset M(R\mathbb{B})$, where $\mathbb{B}$ is a unit ball set. Finally, $M(x)$ is a *convex* set if each point on a line connecting two points in $M(x)$ is also in $M(x)$.

For well-posed hybrid systems there exist several stability and robustness results. First, the notion of stability of sets for a hybrid system is defined:

Definition 3.4.4. *Uniform global pre-asymptopic stability (UGpAS) ([23] Definition 3.6)*
For the hybrid system $\mathcal{H} = (C, F, D, G)$, the closed set $\mathcal{A}$ is said to be

- *uniformly globally stable if there exists a class-$\mathcal{K}_\infty$ function α such that any solution ϕ to $\mathcal{H}$ satisfies $|\phi(t, j)|_\mathcal{A} \leq \alpha(|\phi(0, 0)|_\mathcal{A})$ for all $(t, j) \in dom(\phi)$*
- *uniformly globally pre-attractive if for each $\epsilon > 0$ and $r > 0$ there exists a $T > 0$ such that, for any solution ϕ to $\mathcal{H}$ with $|\phi(0, 0)|_\mathcal{A} \leq r$, $(t, j) \in dom(\phi)$ and $t + j \geq T$ imply $|\phi(t, j)|_\mathcal{A} \leq \epsilon$*
- *uniformly globally pre-asymptotically stable for $\mathcal{H}$ if it is both uniformly globally stable and uniformly globally pre-attractive.*

The distance from a point x to the set $\mathcal{A}$ is defined by $|x|_{\mathcal{A}} := \inf_{y\in\mathcal{A}} |x-y|$. The term *pre-asymptotic* as opposed to asympotic stability and *pre-attraction* as opposed to attraction indicates the possibility of a maximal solution that is not complete.

Similar to classical nonlinear systems theory, Lyapunov functions can be used to analyze stability of sets for hybrid systems.

Definition 3.4.5. *Lyapunov function candidate ([23] Definition 3.16)*
A function $V : dom(V) \mapsto \mathbb{R}$ is said to be a Lyapunov function candidate for the hybrid system $\mathcal{H} = (C, F, D, G)$ if the following conditions hold:

1. *$\bar{C} \cup D \cup G(D) \subset dom(V)$*
2. *V is continuously differentiable on an open set containing $\bar{C}$*

where $\bar{C}$ denotes the closure of C.

Several Lyapunov results exists, next is stated a hybrid Lyapunov theorem which can be used to establish UGpAS of a compact set.

Theorem 1. *Hybrid Lyapunov theorem ([21] Theorem 20)*
Consider the hybrid system $\mathcal{H} = (C, F, D, G)$ satisfying the hybrid basic conditions, and the compact set $\mathcal{A} \subset \mathbb{R}^n$ satisfying $G(\mathcal{A} \cap D) \subset \mathcal{A}$. If there exists a Lyapunov function candidate V for $(\mathcal{H}, \mathcal{A})$ such that

$$\langle \nabla V(x), f \rangle \ < 0 \quad \forall x \in C \setminus \mathcal{A}, f \in F(x) \tag{3.3a}$$

$$V(g) - V(x) < 0 \quad \forall x \in D \setminus \mathcal{A}, g \in G(x) \tag{3.3b}$$

then the set $\mathcal{A}$ is pre-asymptotically stable and the basin of pre-attraction contains every forward invariant compact set.

A consequence of Theorem 2 is that the compact set $\mathcal{A}$ is globally pre-asymptotically stable (GpAS) if $C \cup D$ is compact or the sublevel sets of $V|_{dom(V)\cap(C\cup D)}$ are compact [21]. Furthermore, for systems satisfying the hybrid basic conditions, GpAS is equivalent to UGpAS. For these systems, GpAS also implies robust GpAS. This ensures that vanishing perturbations does not dramatically change the behaviour of solutions.

Next is stated a relaxed version of Theorem 2, which gives sufficient conditions for UGpAS of a non-compact set in the case where there is non-decrease

during jumps, strict decrease during flow, and the duration of flow i sufficiently large. This is the theorem which is used to prove UGpAS of the resetting observer in Paper 2.

Theorem 2. *Sufficient Lyapunov Conditions; Persistent Flowing ([23] Proposition 3.27)*
Let $\mathcal{H} = (C, F, D, G)$ be a hybrid system and let $\mathcal{A} \subset \mathbb{R}^n$ be closed. Suppose V is a Lyapunov function candidate for $\mathcal{H}$ and there exist $\alpha_1, \alpha_2 \in \mathcal{K}_\infty$ and a continuous $\rho \in \mathcal{PD}$ such that

$$\alpha_1(\|x\|_{\mathcal{A}}) \leq V(x) \leq \alpha_2(\|x\|_{\mathcal{A}}) \quad \forall x \in C \cup D \cup G(D) \tag{3.4a}$$

$$\langle \nabla V(x), f \rangle \leq -\rho(\|x\|_{\mathcal{A}}) \quad \forall x \in C, f \in F(x) \tag{3.4b}$$

$$V(g) - V(x) \leq 0 \quad \forall x \in D, g \in G(x) \tag{3.4c}$$

If, for each $r > 0$, there exists $\gamma_r \in \mathcal{K}_\infty$, $N_r > 0$ such that for every solution ϕ to $\mathcal{H}$, $\|\phi(0,0)\|_{\mathcal{A}} \in (0, r]$, $(t, j) \in dom(\phi)$, $t + j \geq T$ imply $t \geq \gamma_r - N_r$, then $\mathcal{A}$ is uniformly globally pre-asymptotically stable for $\mathcal{H}$.

Chapter 4

Case study: Autonomous docking of the double-ended car ferry MF Gloppefjord

In this chapter, a case study is conducted with autonomous docking of a double-ended car ferry. In the docking control system both the control allocation from Paper 1 and the observer from Paper 2 are in the loop. This aims to illustrate how these can be utilized in a ferry control system, and to supplement the results given in the papers.

4.1 The Anda-Lote crossing

The case used in the simulator is the stretch across Nordfjorden between Anda and Lote at the west coast of Norway. The duration of the crossing is 11 minutes, with departures every 20 minutes from each side. The site is operated by Fjord1 AS.

Figure 4.1: The ferry strech between Anda and Lote. Source: www.1881.no

The Anda-Lote site features several innovations. One is the fully automated charging and docking tower delivered by Stemmann and Cavotec. The tower includes a robotic arm which grabs the ferry and pulls it to the dock using a vacuum pad, and connects to a charger. See Figure 4.2.

Figure 4.2: The charging tower "FerryCharger" and automated docking solution at the Anda-Lote site. Source: Teknisk Ukeblad

The environmental conditions at Anda-Lote are harsh. The site is located deep within the narrow Norwegian fjords, and is therefore sheltered from waves. However, it is exposed to strong cross-currents and winds [33].

4.2 MF Gloppefjord

The ferries that operate the Anda-Lote site are the sister ships MF Gloppefjord and MF Eidsfjord. The main characteristics of the ferries are given in Table 4.1.

Table 4.1: Main characteristics of MF Gloppefjord. Source: [33]

Characteristic	**Value**
Delivered year	2017
Carrying capacity	120 cars + 349 passangers
Length between perpendiculars	102.6m
Length overall	106.0m
Breadth	17.2m
Draft	3.8m
Thrusters	2 x 900kW Azipull
Battery capacity	2 x 540kWh

The ferries have a standard design for double-ended car ferries, with fore-aft symmetry in both the hull and the thruster configuration. The ferries also have an automated crossing system delivered by Rolls-Royce Marine AS.

4.3 Simulator setup

The simulator used in the case study was developed by the author in [36]. It is based on a *SINTEF Ocean VeSim* vessel model for a generic double-ended car ferry, kindly provided by Rolls-Royce Marine AS. The vessel model uses numerical hydrodynamic calculations from well known software, such as Veres and HullVisc. The vessel simulator features:

- A unified maneuvering and seakeeping model
- User provided thruster models
- Environmental loads including current forces, dynamic wind loads from several wind spectra, and first and second order wave loads from several wave spectra.

For rapid development and testing of control systems, *MathWorks Simulink*, is well suited. With this in mind, a custom interface from VeSim to Simulink was created.

In Simulink, sensor models were developed, as shown in Figure 4.3. They include:

- A GNSS model, implemented by adding Gaussian white noise to the true North, East and Down positions from the vessel simulator.
- A compass model, implemented by adding Gaussian white noise to the true heading angle from the vessel simulator.
- An IMU model based on the Simulink "Three-Axis Inertial Measurement Unit" block [39]. This model includes sensor noise for the accelerometers and rate gyros, sensor bias for the rate gyros and second order sensor dynamics for the acceleromers and rate gyros. Linking this sensor model to the VeSim model required some preprossesing of signals. BODY frame acceleration from VeSim was obtained, and added to a coriolis term calculated by the true angular and linear velocities of the vessel. The resulting acceleration was input to the IMU sensor model. The true vessel attitude was also obtained, and the NED frame gravitational acceleration was transformed to the BODY frame using this attitude. The resulting BODY frame gravitational acceleration was also input to the IMU sensor model.

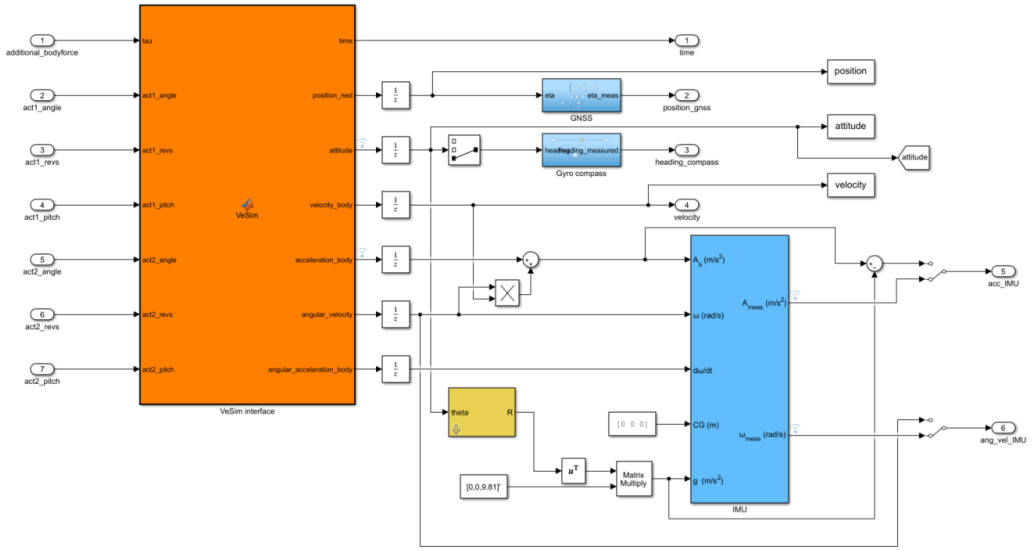

Figure 4.3: Implementation of Simulink interface with sensor models

The implementation shown in Figure 4.3 is wrapped by a final block, only interfacing the inputs and outputs that are available in a real vessel control

system. The inputs are the thruster setpoints, that is, speed, pitch and angle for each of the azimuth thrusters. The outputs are the measurements from the sensor models. The final block is shown in Figure 4.4.

Figure 4.4: Simulink block for the VeSim interface

In [36] a complete control system for the crossing, transition and docking modes of operation was developed. This system utilizes all the components from Chapter 2 with some additional novelties. It also includes a hybrid supervisor to switch between modes and synchronize the states after a switch. The reader is referred to [36] for details on this control system.

In this case study, only the docking mode of operation is considered. The control system will reuse some components from the original system, while introducing the control allocation algorithm and observer from Paper 1 and 2. For clarity, the components used in the control loop in this case study is listed here:

- Control allocation from Paper 1
- Resetting observer from Paper 2

- DP controller from Section 2.3.1
- Reference filter guidance law from Section 2.4.2

All parameters used in the case study are given in Appendix A.

4.4 Simulation results and discussion

In this section, the results from the case study is presented and discussed along the way. Because the control allocation algorithm is tested extensively in the same simulator in [36], the focus on this case study is on the resetting observer. However, the control allocation algorithm from Paper 1 is in the loop in all simulations, and the interactions between the allocation, the resetting observer and the rest of the control system is therefore tested.

The case study is divided into three sub-cases. First, a nominal case is included with no external disturbances and sensor noise. Then, a case where the ferry is subject to a sudden lateral pulse disturbance is tested. This is a highly relevant case for docking of car ferries, as they often experience a sudden change in cross-current when they approach the dock [36]. Finally, also sensor noise is included to investigate how this affects the resetting observer.

The trajectory used in all cases is sampled from the actual approach to the Anda dock used by MF Gloppefjord. The ferry starts with an initial surge speed of $2m/s$. In all cases, two simulations are run. One with the resetting observer in the loop and one with a continuous-time observer in the loop, for comparison. The continuous-time observer is identical to the resetting observer minus the resetting mechanism. This is the equivalent to the observer of (2.19), not including the wave-frequency model.

4.4.1 Nominal case

In the nominal case, the vessel is not subject to any external disturbances or measurement noise. Figure 4.5 shows the reference trajectory together with the actual trajectories when using the continuous observer and the resetting observer in the loop. The results show that the ferry tracks the reference trajectory well with both observers. Some minor oscillations are present for

the continuous-time observer.

Figure 4.6 and 4.7 shows the velocity estimates from the continuous-time observer and the resetting observer, respectively. The results show that the continuous-time observer is able to estimate the velocities quite well. This is as expected, because in this nominal case the model used in the observer matches well with the actual behaviour. Hence, the observer is not reliant on the slow position measurement injection dynamics to estimate the velocity. During the most rapid changes in velocity there are some offsets, and this likely causes the oscillations that can be observed in the actual velocity. The resetting observer estimates the velocities very well, and the results show that this has a noticeable effect on the actual vessel velocities.

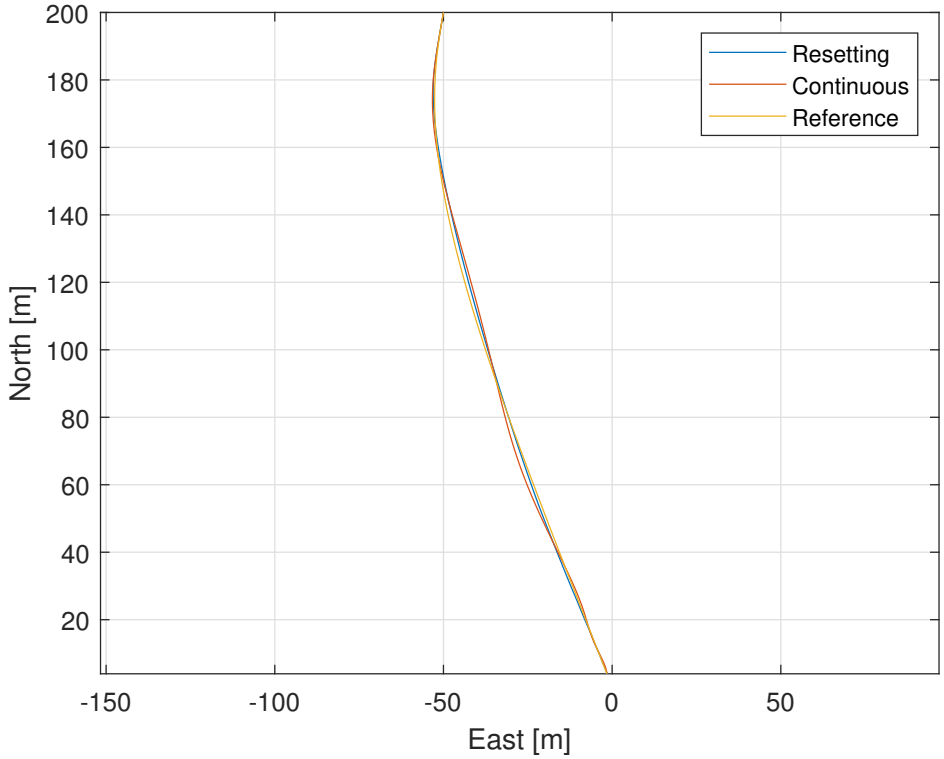

Figure 4.5: Trajectory for the nominal case

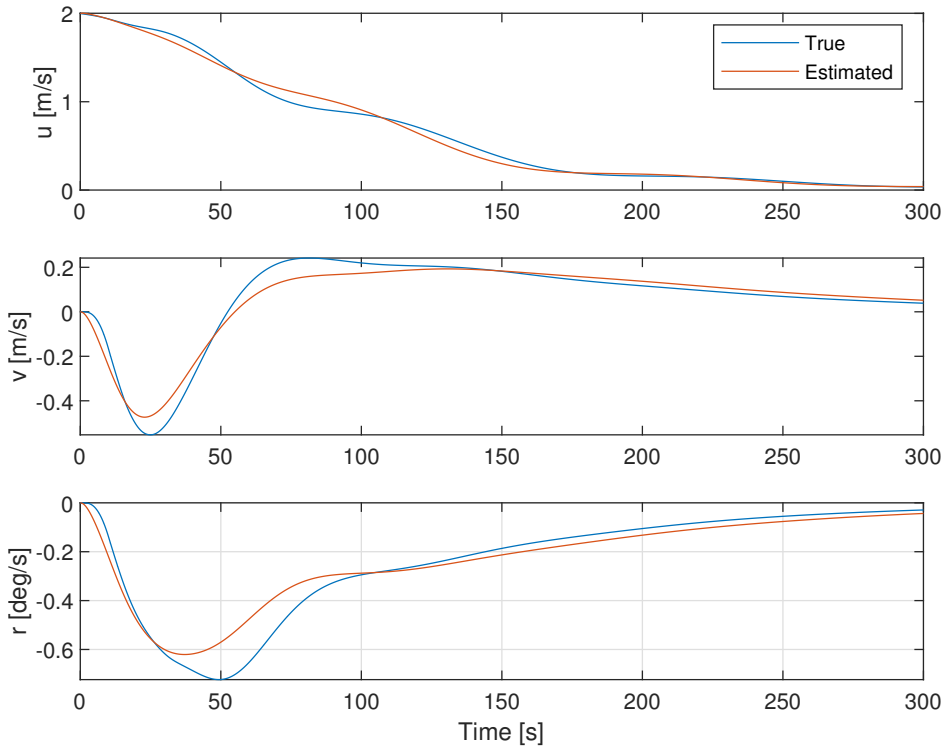

Figure 4.6: Velocity estimates for the continuous observer in the nominal case

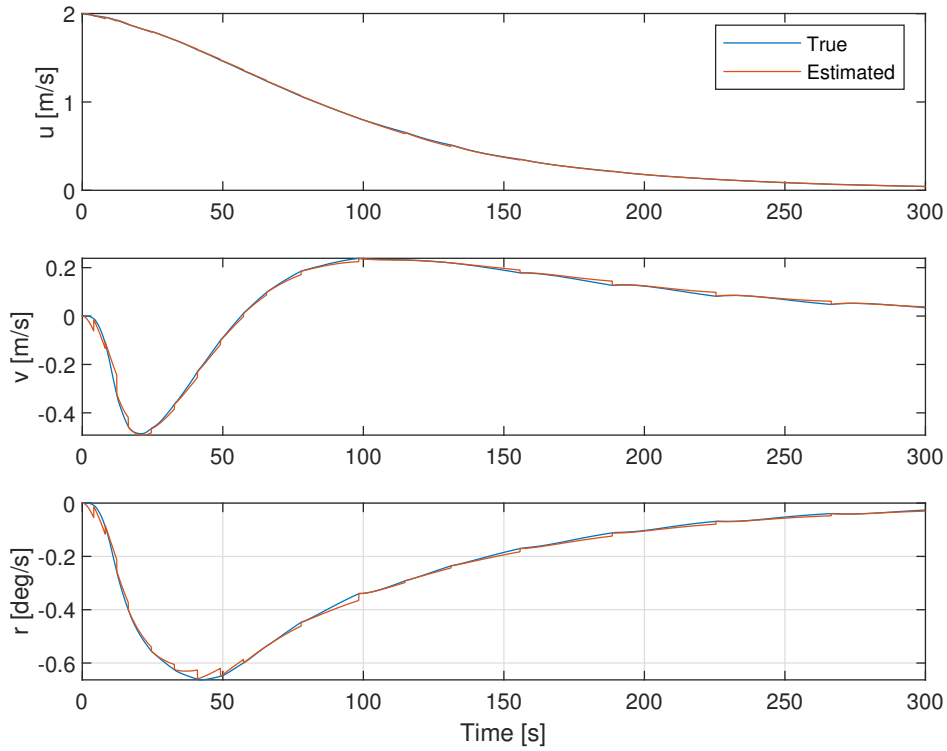

Figure 4.7: Velocity estimates for the resetting observer in the nominal case

4.4.2 Lateral disturbance

In this case, the ferry is subject to a lateral pulse load of $200kN$ with a duration of $20s$. The pulse starts at simulation time $t = 50s$.

Figure 4.8 shows the reference trajectory together with the actual trajectories when using the continuous-time observer and the resetting observer in the loop. The figure shows that the disturbance has a profound affect on the ferry's trajectory. However, when using the resetting observer, there is only a small initial offset before the ferry converges back to the reference. When using the continuous-time observer, large and sustained oscillations are present.

Figure 4.9 and 4.10 provides an explanation for the observed behaviour in Figure 4.8. Where the resetting observer captures the transient sway velocity induced by the disturbance well, the continuous-time observer barely responds to it at all.

Figure 4.11 shows the desired thrust from the DP controller together with the actual generated thrust by the azimuth thrusters. It compares the thrust when using the resetting and the continuous-time observer in the loop. The figure shows that when using the resetting observer, the controller commands a short burst of sway thrust to counteract the disturbance and push the ferry back to the reference. Not surprisingly, the figure also shows that the resetting observer introduces some jumps in the thrust. This might in some cases produce angle and speed references for the thrusters which are difficult to follow. This is apparent in Figure 4.11 at $t = 60s$. The large jump in desired sway thrust causes a spike in the produced yaw moment. This occurs because the thrusters have much faster speed dynamics than angle dynamics. When a large jump in sway thrust is requested, the thrusters therefore start producing thrust before the servos have had the time to turn to the desired angle, and therefore produces an incorrect yaw moment for a brief moment. Apart from this, the control allocation results in thrust that closely matches the desired thrust.

Figure 4.11 also shows that the thrust usage is reduced when using the resetting observer, due to the lack of oscillations. However, when using the resetting obsever it is clear that the thrust varies more than when using the continuous-time observer. Due to the inertia of the propeller, drive train and

the surrounding water, it requires energy change thrust. This is not reflected by only investigating thrust curve. A relevant topic of future research is to include a propeller-shaft model and compare the actual energy usage for these two observers.

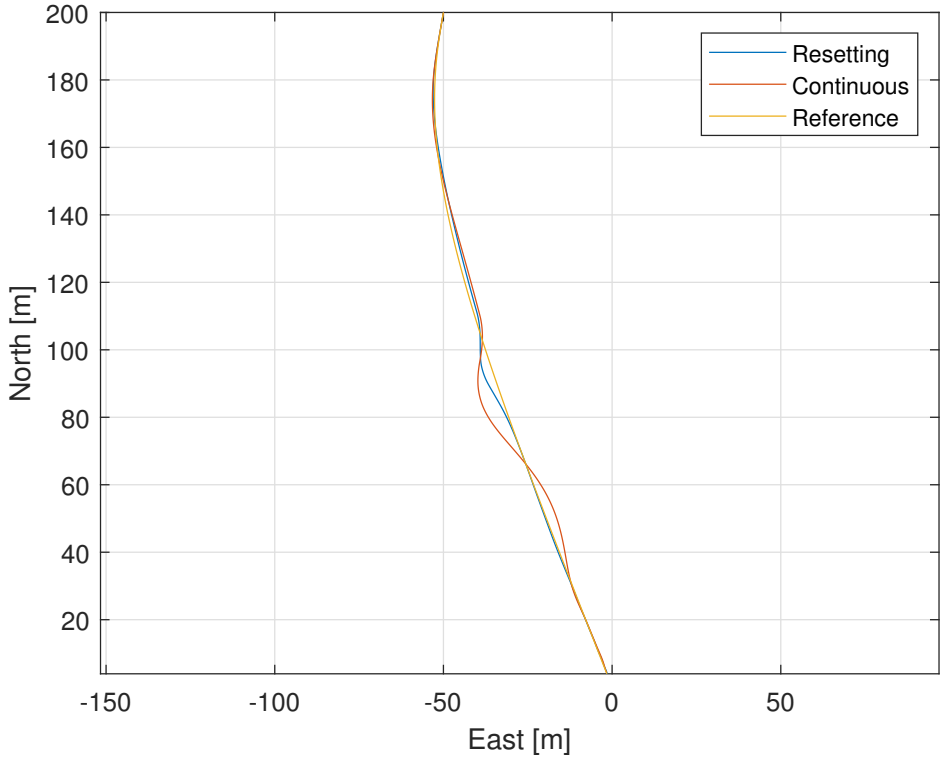

Figure 4.8: Trajectory for the nominal case

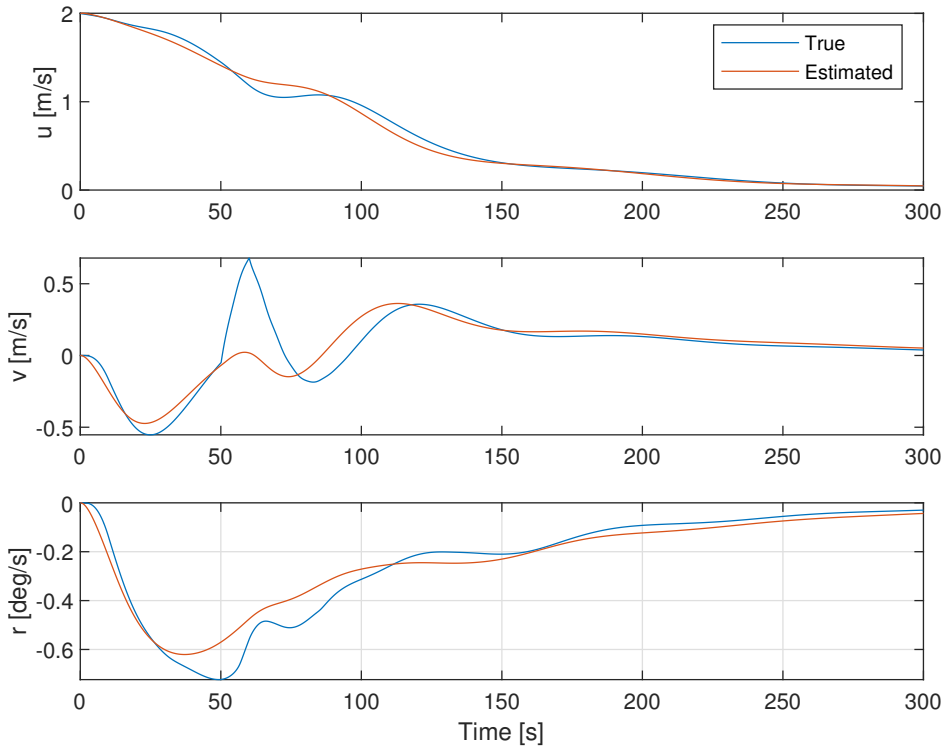

Figure 4.9: Velocity estimates for the continuous observer with lateral disturbance

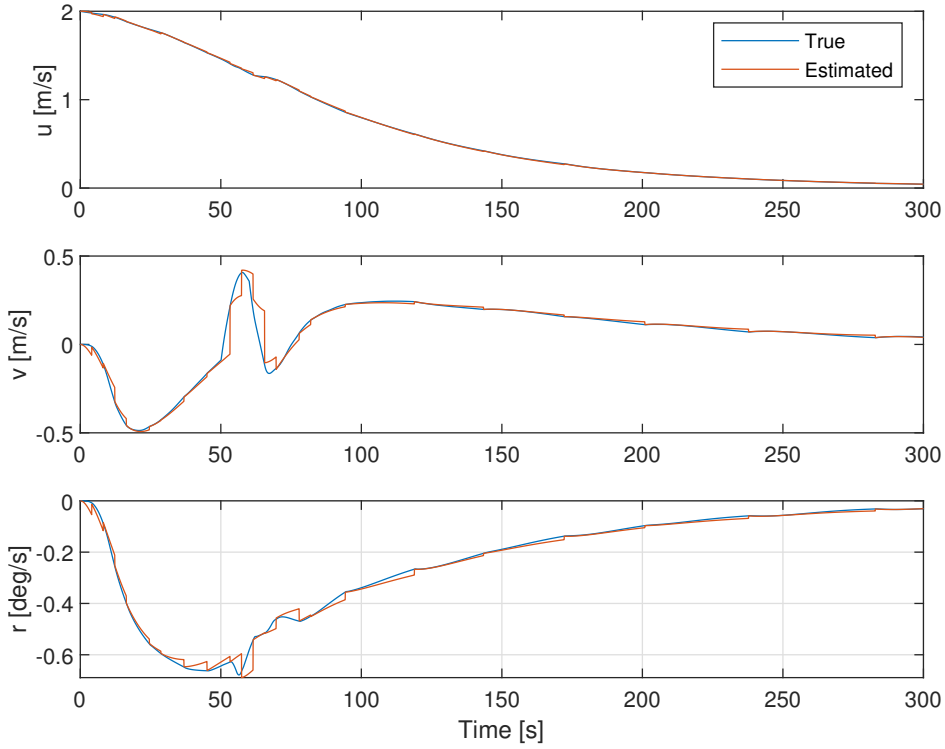

Figure 4.10: Velocity estimates for the resetting observer with lateral disturbance

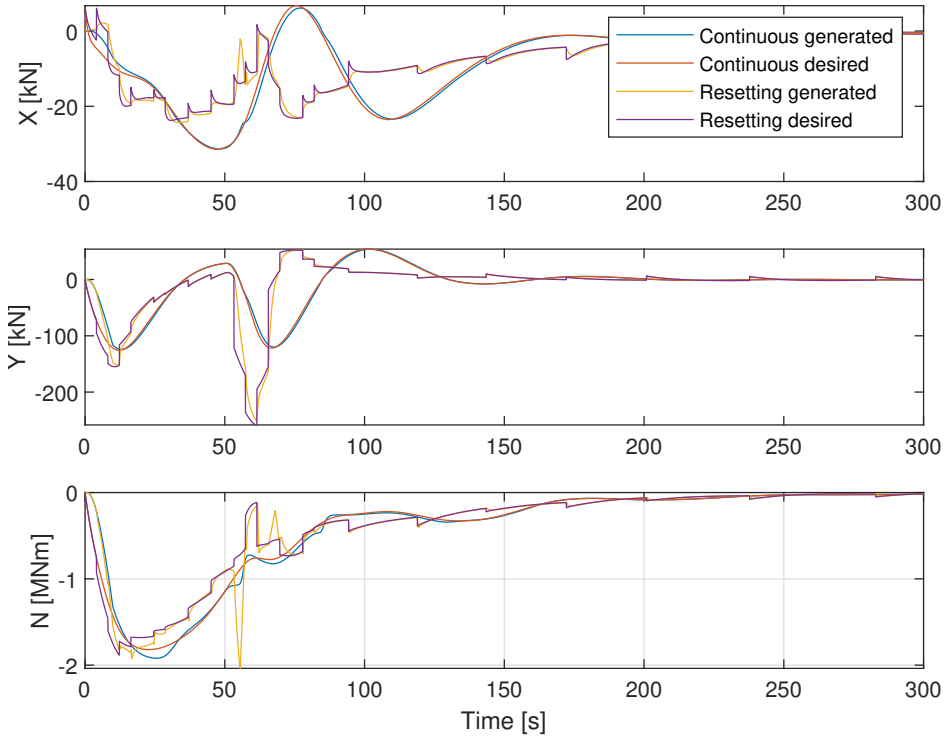

Figure 4.11: Desired and generated thrust for both observers with lateral disturbance

4.4.3 Measurement noise

In the final case, measurement noise is added to the position and heading measurements which are injected into the observers. This aims to investigate how the resetting observer performs under measurement noise. The lateral disturbance of Section 4.4.2 is still present.

Figure 4.12 shows the velocity estimates for the resetting observer. The results show that the resetting mechanism is not much affected by the noise when comparing to the noise-free case of Figure 4.10. Also the thrust plot of Figure 4.13 confirms this.

As discussed in Paper 2, a linear interpolation between the pre- and post-jump estimates is added to the jump map. The provides the user with some tuning flexibility in case of high-noise conditions where the jumps might not produce accurate estimates. For this case, the interpolation was not necessary because the jumps produces highly accurate estimates. Another consideration to be aware of, is that the estimation error bounds, which triggers a jump, should be set larger than the expected noise standard deviation. This is to ensure that the noise does not trigger unwanted jumps.

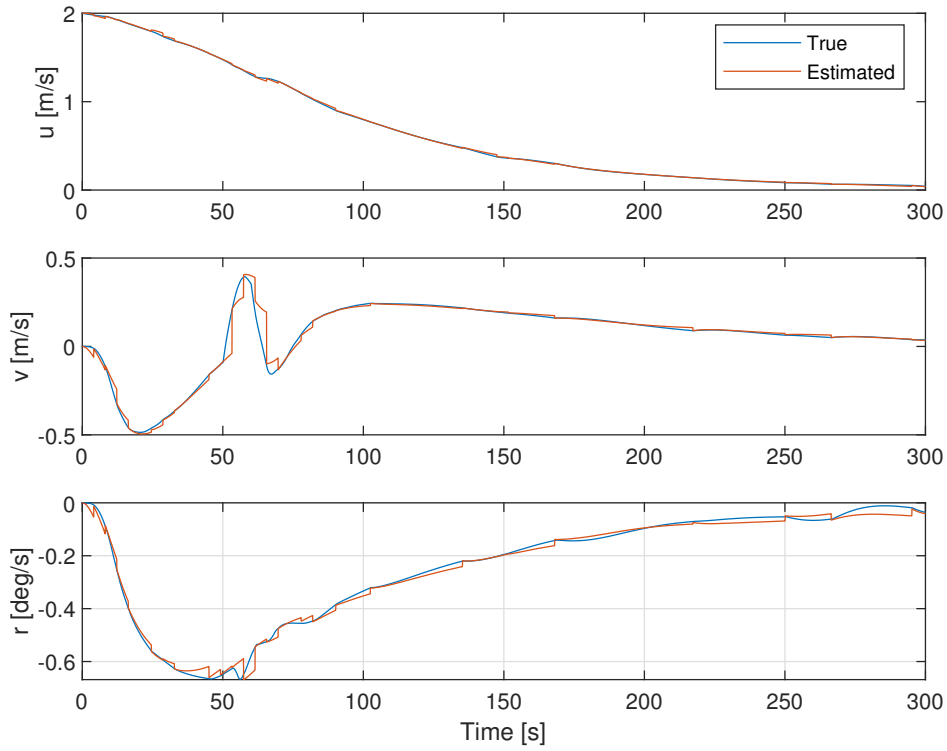

Figure 4.12: Velocity estimates for the resetting observer with lateral disturbance and measurement noise

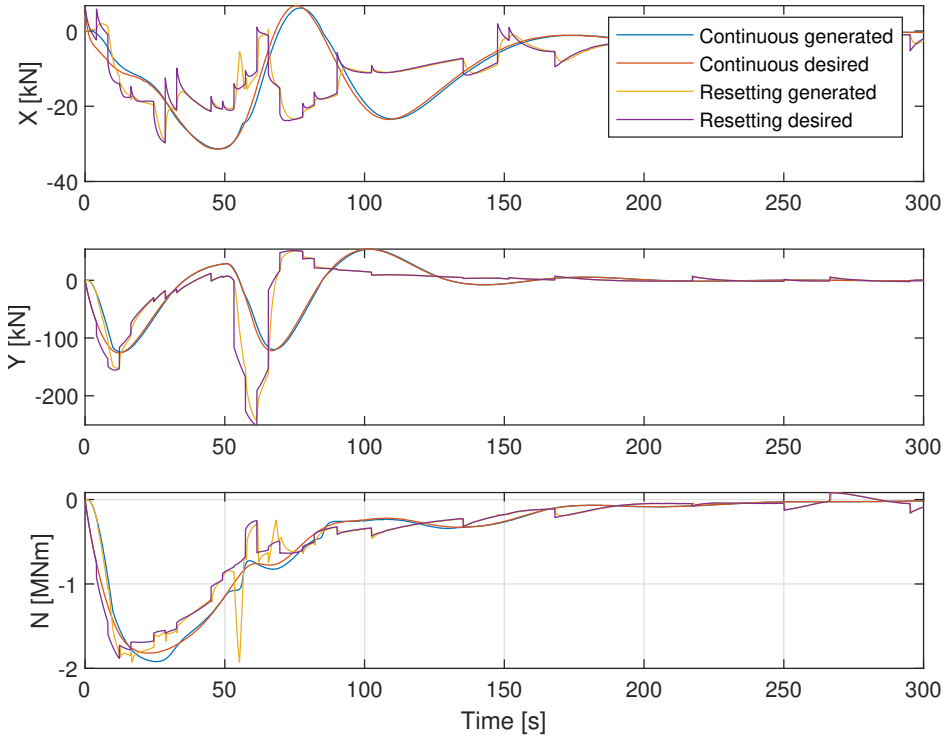

Figure 4.13: Desired and generated thrust for both observers with lateral disturbance and measurement noise

Chapter 5

Conclusions and further work

5.1 Concluding remarks

In this thesis, two papers on topics related to control of autonomous ferries have been presented, and a case study integrating results from both papers has been conducted.

The topic of Paper 1 is control allocation for double-ended ferries with symmetric thruster configuration. The allocation problem is formulated as a nonlinear optimization problem. The paper presents a reformulation of the original problem which transforms it into a bounded, scalar optimization problem. The algorithms is tested in simulation with a car ferry and in full-scale experiments with a passenger ferry. The simulation results show good coherence between commanded and produced thrust compared with existing methods. The experimental results demonstrate good DP performance. The computational complexity was also compared with a quadratic programming (QP) method. By generating 20 000 samples, a distribution of the elapsed time for one iteration was formed. The results show that the mean elapsed time for the novel allocation was 37.8 times lower than for the QP allocation. The former also had a much more narrow distribution, which is a desired property for use in a real-time control system. In total, these results give confidence in the novel allocation algorithm for use in control of autonomous ferries.

The topic of Paper 2 is observer design. The paper presents a resetting ob-

server for linear time-varying systems. A reset in the state estimate is triggered if the output estimation error exceeds predefined bounds. To calculate the new state estimates after a jump, an approach inspired from finite-time observer design is used. The finite-time equations are derived for linear time-varying systems and a method for online calculation of the state transition matrices is presented. The observer equations are formulated in the hybrid dynamical systems framework of Section 3.4, and sufficient conditions for Uniform Global pre-Asymptotic Stability (UGpAS) is given. The observer can be applied to generic observable linear-time varying systems, but has particularly interesting applications to dynamic positioning of marine surface vessels. A simulation study with observer design for a offshore support vessel was conducted. The results show great improvements in the reactivity to unmodelled disturbances compared to a continuous-time observer, without compromising steady-state performance. By adding a notch-filter at the input of the observer, good performance in waves was also achieved.

Finally, a case study with autonomous docking for a double-ended car ferry was conducted. This simulation study used both the control allocation from Paper 1 and the resetting observer from Paper 2 in the control loop. The behaviour when using the resetting observer versus a continuous-time observer was compared. The case study was divided into three sub-cases. First, a nominal case with no external disturbances or measurement noise. Here, both observers produced good state-estimates, resulting in good tracking of the desired trajectory towards the dock. In the second case, the ferry was subject to a sudden lateral disturbance pulse. In this case, the continuous-time observer was not able to capture the resulting rapid change in sway velocity, resulting in large deviations from the reference trajectory and sustained oscillations. The resetting observer captured the change in sway velocity well, and the ferry quickly converged back to the reference trajectory after an initial offset. Comparing the thrust usage for the two observers, it is apparent that the resetting observer uses less thrust. However, the resetting introduces some jumps in the thrust, which may be unfortunate for fuel-economy and wear-and-tear. In the final case, measurement noise was added to the position and heading measurements. The results show that the resetting observer is not much affected by the noise, and still produces good state estimates.

5.2 Further work

The control allocation algorithm of Paper 1 has been tested both in simulation and in full-scale experiments. It has also been used actively in the autonomous passenger ferry milliAmpère [40] for more than a year. This algorithm is thus quite mature. The resetting observer, on the other hand, is still at an early research stage. Several topics for further work exist.

Paper 2 highlights the need for further work on the theoretical foundations of the observer. In particular, relaxed conditions for asymptotic stability should be investigated. The sufficient conditions given are likely highly conservative, and this makes it difficult to find a tuning and a corresponding Lyapunov function to ensure a decrease in the Lyapunov function after a jump. In the case study of this thesis, the interpolation matrix, K, in the jump map was set to identity, making the stability analysis trivial.

Conditions for non-singularity of the term $(I - \Phi_1\Phi_2^{-1})$ in the jump map should also be investigated. The discussion in Paper 2 highlights some possible approaches.

The discussion in Section 4.4 calls out for simulation studies including a propeller-shaft model, to investigate how the jumps in the thrust due to the resetting affects fuel consumption due to acceleration and deceleration of the propeller and drive-train. Experimental results with the observer should also be carried out, to build confidence in the methodology.

Finally, the resetting observer is a method which can be applied to generic linear time-varying systems. An interesting topic for future work find other applications for such a low-gain - high reactivity observer, and evaluate its usability and performance there.

Bibliography

[1] H. S. Witsenhausen, "A Class of Hybrid-State Continuous-Time Dynamic Systems," *IEEE Transactions on Automatic Control*, vol. 11, no. 2, 1966, ISSN: 15582523. DOI: 10.1109/TAC.1966.1098336.

[2] J. G. Balchen, N. A. Jenssen, E. Mathisen, and S. Sælid, "A dynamic positioning system based on Kalman filtering and optimal control," *Modelling, Identification and Control*, vol. 1, no. 3, pp. 135–163, 1980.

[3] L. Tavernini, "Differential automata and their discrete simulators," *Nonlinear Analysis: Theory, Methods & Applications*, vol. 11, no. 6, pp. 665–683, 1987, ISSN: 0362546X. DOI: 10.1016/0362-546X(87)90034-4.

[4] S. Salcudean, "A Globally Covergent Angular Velocity Observer for Rigid Body Motion," *IEEE Transactions on Automatic Control*, vol. 36, no. 12, pp. 1493–1497, 1991.

[5] A. Back, J. Guckenheimer, and M. Myers, "A dynamical simulation facility for hybrid systems," in *International Hybrid Systems Workshop*, 1992, pp. 255–267, ISBN: 038757318. DOI: 10.1007/3-540-57318-6{_}32. [Online]. Available: http://link.springer.com/10.1007/3-540-57318-6_32.

[6] P. Antsaklis, J. Stiver, and M. Lemmon, "Hybrid system modeling and autonomous control systems," in *International Hybrid Systems Workshop*, 1993, pp. 366–392. [Online]. Available: http://www.springerlink.com/index/p62226341550744t.pdf.

[7] A. Nerode and W. Kohn, "Models for hybrid systems : automata, topologies, controllability, observability," *Hybrid Systems, Lecture Notes in Computer Science*, pp. 317–356, 1993. DOI: 10.1007/3-540-57318-6{_}35.

[8] M. S. Branicky, "Studies in Hybrid Systems: Modeling, Analysis, and Control," PhD thesis, MASSACHUSETTS INSTITUTE OF TECHNOLOGY, 1995.

[9] O. Faltinsen, *Sea loads on ships and offshore structures*. 1998, ISBN: 0-521-45870-6. DOI: 9780521458702.

[10] R. T. Rockafellar and R. J.-B. Wets, *Variational Analysis*. 1998, ISBN: 9783540627722. DOI: 10.1021/jp7118845.

[11] J. P. Fossen T. I. & Strand, "Passive nonlinear observer design for ships using Lyapunov methods," *Automatica*, vol. 35, no. 1, pp. 3–16, 1999.

[12] J. Hespanha, "Tutorial on supervisory control," *Lecture Notes for the workshop Control using Logic and Switching for the 40th Conf. on Decision and Contr.*, pp. 1–46, 2001.

[13] B. Vik, "A nonlinear observer for GPS and INS integration," in *Proceedings of the 40th IEEE Conference on Decision and Control*, 2001, ISBN: 0780370619. DOI: 10.1109/.2001.980726. [Online]. Available: http://ieeexplore.ieee.org/xpls/abs_all.jsp?arnumber=980726.

[14] J. P. Hespanha and A. S. Morse, "Switching between stabilizing controllers," *Automatica*, vol. 38, no. 11, pp. 1905–1917, 2002, ISSN: 00051098. DOI: 10.1016/S0005-1098(02)00139-5.

[15] H. K. Khalil, "Nonlinear Systems," *Prentice-Hall, New Jersey*, 2002, ISSN: 0949-1775. DOI: 10.1007/978-1-4757-3108-8.

[16] J. P. Hespanha, "Hysteresis-based switching algorithms for supervisory control of uncertain systems Hysteresis-based switching algorithms for supervisory control of uncertain systems," *University of California Postprints*, vol. 39, pp. 263–272, 2003.

[17] T. I. Fossen and T. A. Johansen, "A survey of control allocation methods for ships and underwater vehicles," *14th Mediterranean Conference on Control and Automation, MED'06*, pp. 1–6, 2006, ISSN: 1098-0121. DOI: 10.1109/MED.2006.328749.

[18] T. D. Nguyen, A. J. Sørensen, and S. Tong Quek, "Design of hybrid controller for dynamic positioning from calm to extreme sea conditions," *Automatica*, vol. 43, no. 5, pp. 768–785, 2007, ISSN: 00051098. DOI: 10.1016/j.automatica.2006.11.017.

[19] R. Mahony, T. Hamel, and J.-M. Pfimlin, "Nonlinear Complementary Filters on the Special Orthogonal Group," *IEEE Transactions on Automatic Control*, vol. 53, no. 5, pp. 1203–1218, 2008, ISSN: 00207179. DOI: 10.1109/TAC.2008.923738.

[20] T. D. Nguyen, A. J. Sørensen, and S. T. Quek, "Multi-operational controller structure for station keeping and transit operations of marine vessels," *IEEE Transactions on Control Systems Technology*, vol. 16, no. 3, pp. 491–498, 2008, ISSN: 10636536. DOI: 10.1109/TCST.2007.906309.

[21] R. Goebel, R. G. Sanfelice, and A. R. Teel, "Hybrid dynamical systems," *IEEE Control Systems Magazine*, vol. 29, no. 2, pp. 28–93, 2009, ISSN: 08880611. DOI: 10.1109/MCS.2008.931718.

[22] T. I. Fossen, *Handbook of Marine Craft Hydrodynamics and Motion Control*. Wiley, 2011, ISBN: 978-1-119-99149-6.

[23] R. Goebel, R. G. Sanfelice, and A. R. Teel, *Hybrid Dynamical Systems : Modeling, Stability, and Robustness.* Princeton University Press, 2012, p. 227, ISBN: 1400842638. [Online]. Available: https://books.google.no/books?hl=en&lr=&id=JwrOY03fuGQC&oi=fnd&pg=PP1&dq=info:Tl8gDI0O3QEJ:scholar.google.com&ots=TpU8ELWhbC&sig=r7zQ6kma2MhE_uw-qkAhnS2oQNI&redir_esc=y#v=onepage&q&f=false.

[24] H. F. Grip, T. I. Fossen, T. A. Johansen, and A. Saberi, "Nonlinear observer for GNSS-aided inertial navigation with quaternion-based attitude estimation," *2013 American Control Conference*, pp. 272–279, 2013, ISSN: 07431619. DOI: 10.1109/ACC.2013.6579849. [Online]. Available: http://ieeexplore.ieee.org/document/6579849/.

[25] T. A. Johansen and T. I. Fossen, "Control allocation - A survey," *Automatica*, vol. 49, no. 5, pp. 1087–1103, 2013, ISSN: 00051098. DOI: 10.1016/j.automatica.2013.01.035.

[26] T. Bryne, T. I. Fossen, and T. A. Johansen, "A Virtual Vertical Reference Concept for for Applications Sea Surface Applications at the GNSS / INS Applications at the Sea Surface," *IFAC-PapersOnLine*, vol. 48, no. 16, pp. 127–133, 2015, ISSN: 2405-8963. DOI: 10.1016/j.ifacol.2015.10.269. [Online]. Available: http://dx.doi.org/10.1016/j.ifacol.2015.10.269.

[27] D. De Almeida Fernandez, *An output feedback motion control system for ROVs: Guidance, navigation and control*, June. 2015, ISBN: 9788232609000.

[28] H. F. Grip, T. I. Fossen, T. A. Johansen, and A. Saberi, "Globally exponentially stable attitude and gyro bias estimation with application to GNSS/INS integration," *Automatica*, vol. 51, pp. 158–166, 2015, ISSN: 00051098. DOI: 10.1016/j.automatica.2014.10.076. [Online]. Available: http://dx.doi.org/10.1016/j.automatica.2014.10.076.

[29] T. H. Bryne and T. I. Fossen, "Introductory Lecture Notes on Aided Inertial Navigation Systems," no. August, 2016.

[30] W. Caharija, K. Y. Pettersen, M. Bibuli, P. Calado, E. Zereik, J. Braga, J. T. Gravdahl, A. J. Sørensen, M. Milovanović, and G. Bruzzone, "Integral line-of-sight guidance and control of underactuated marine vehicles: Theory, simulations and experiments," *IEEE Transactions on Control Systems Technology*, vol. 24, no. 5, pp. 1623–1642, 2016.

[31] G. I. Bitar, *Towards the Development of Autonomous Ferries*. Department of Engineering Cybernetics. Norwegian University of Science and Technology (NTNU), Trondheim: Master thesis, 2017.

[32] S. Skjong and E. Pedersen, "Nonangular MPC-Based Thrust Allocation Algorithm for Marine Vessels - A Study of Optimal Thruster Commands," *IEEE Transactions on Transportation Electrification*, vol. 3, no. 3, pp. 792–807, 2017, ISSN: 23327782. DOI: 10.1109/TTE.2017.2688183.

[33] Tore Stensvold, *Dette er verdens første helelektriske fergesamband - Tu.no*, 2017. [Online]. Available: https://www.tu.no/artikler/dette-er-verdens-forste-helelektriske-fergesamband/438991?key=IfQmbvmi.

[34] A. H. Brodtkorb, S. A. Værnø, A. R. Teel, A. J. Sørensen, and R. Skjetne, "Hybrid controller concept for dynamic positioning of marine vessels with experimental results," *Automatica*, vol. 93, pp. 489–497, 2018, ISSN: 00051098. DOI: 10.1016/j.automatica.2018.03.047. [Online]. Available: https://doi.org/10.1016/j.automatica.2018.03.047.

[35] A. J. Sørensen, *Marine Cybernetics*. 2018.

[36] T. R. Torben, *Hybrid Control of Autonomous Ferries*, December. Department of Marine Technology. Norwegian University of Science and Technology (NTNU), Trondheim: Project thesis, 2018. DOI: 10.13140/RG.2.2.10564.88969.

[37] Bastø Fosen, *Samarbeider om teknologi til fremtidens ferger - Bastø Fosen*. [Online]. Available: http://basto-fosen.no/nyheter/samarbeider-om-teknologi-til-fremtidens-ferger-article3399-132.html.

[38] *History of Computers and Computing, Birth of the modern computer, The bases of digital computers, relay*. [Online]. Available: http://history-computer.com/ModernComputer/Basis/relay.html.

[39] *Implement three-axis inertial measurement unit (IMU) - Simulink*. [Online]. Available: https://www.mathworks.com/help/aeroblks/threeaxisinertialmeasurementunit.html.

[40] T. Stensvold, *Asia kommer for fullt. Vi havner bakpå om vi ikke gir gass*. [Online]. Available: https://www.tu.no/artikler/ntnu-autonomi-er-en-stor-satsing-for-oss-vi-har-100-som-tar-doktorgraden/440081?key=EWNVcNHQ.

[41] ——, *Nå er MF Folgefonn verdens første fartøy med automatisk dokking*. [Online]. Available: https://www.tu.no/artikler/na-er-mf-folgefonn-verdens-forste-fartoy-med-automatisk-dokking/435810?key=cDVcEUuO.

Appendix A

Parameters

This appendix contains the numerical values of the parameters used in the simulation study.

Table A.1: Parameters for MF Gloppefjord case study. Part 1

Parameter	**Value**
Observer paramters	
Injection gain for z_1 position	$\begin{pmatrix} 1.1 & 0 & 0 \\ 0 & 1.1 & 0 \\ 0 & 0 & 1.1 \end{pmatrix}$
Injection gain for z_1 bias	$\begin{pmatrix} 0.003 & 0 & 0 \\ 0 & 0.003 & 0 \\ 0 & 0 & 0.003 \end{pmatrix}$
Injection gain for z_1 velocity	$\begin{pmatrix} 0.03 & 0 & 0 \\ 0 & 0.03 & 0 \\ 0 & 0 & 0.03 \end{pmatrix}$
Injection gain for z_2 position	$\begin{pmatrix} 0.77 & 0 & 0 \\ 0 & 0.77 & 0 \\ 0 & 0 & 0.77 \end{pmatrix}$
Injection gain for z_2 bias	$\begin{pmatrix} 0.15 & 0 & 0 \\ 0 & 0.15 & 0 \\ 0 & 0 & 0.15 \end{pmatrix}$
Injection gain for z_2 velocity	$\begin{pmatrix} 1.5 & 0 & 0 \\ 0 & 1.5 & 0 \\ 0 & 0 & 1.5 \end{pmatrix}$
Reset interval	$4.0s$
Estimation error bounds	$[0.01m, 0.01m, 0.001rad]$
Interpolation matrix	$I_{9\times 9}$

Table A.2: Parameters for MF Gloppefjord case study. Part 2

Parameter	**Value**
Controller parameters	
Docking controller natural period	$50s$
Docking controller damping ratio	1.0
Docking controller integral gain	$K_p \frac{2\pi}{10T_n}$
Control plant model damping matrix	$\begin{pmatrix} 3.2 \times 10^3 & 0 & 0 \\ 0 & 1.5 \times 10^5 & 0 \\ 0 & 0 & 1.5 \times 10^8 \end{pmatrix}$
Control plant model mass matrix	$\begin{pmatrix} 1.5 \times 10^6 & 0 & 0 \\ 0 & 2.4 \times 10^6 & 0 \\ 0 & 0 & 1.5 \times 10^9 \end{pmatrix}$
Guidance paramters	
Reference filter natural frequency	0.05
Reference filter damping ratio	2.0
Thruster model parameters	
Max thrust	$200kN$
Thrust time constant	$1.5s$
Max turn rate servo	$12\frac{deg}{s}$
Distance from thruster to vessel center	$45m$
Sensor model parameters	
Noise variance GNSS	$1 \times 10^{-5} m^2$
Noise variance heading compass	$1 \times 10^{-8} rad^2$
Noise sample time	$0.1s$

Appendix B

Cost function for control allocation

In this appendix the implementation of the cost function used in the control allocation is given. This serves to show the exact for of the cost function that is used, motivate how a cost function for this algorithm might look and to document the parameters used.

```
%% Cost function
function cost = cost_fcn_docking(Fx1, Fy1, Fy2, tau_x,
    F1_last, F2_last, a1_last, a2_last)
    %Weights. Angles i deg, thrust i kN
    a = [10 10];%Cost of change of angle
    b = [0.1 0.1];%Cost of thrust usage
    c = [0.1 0.1];%Cost of thrust change
    d = [3 3];%Cost of deviation from home angle
    e = [0.1 0.1];%Cost of deviation from mean thrust

    home_angle = [180 0];
    mean_thrust = [50 50];

    %Calculate thrust and change of angle, convert to
       degs and kN;
    Fx1 = min(-eps, Fx1);
    Fx2 = tau_x - Fx1;
    a1 = atan2(Fy1,Fx1);
    a2 = atan2(Fy2,Fx2);
    F1 = sqrt(Fx1^2 + Fy1^2)*1e-3;
    F2 = sqrt(Fx2^2 + Fy2^2)*1e-3;
    move1 = shortest_angle_path(a1_last,a1)*180/pi;
    move2 = shortest_angle_path(a2_last,a2)*180/pi;
    F1_last = F1_last*1e-3;
    F2_last = F2_last*1e-3;
    angle_dev1 = shortest_angle_path(deg2rad(home_angle
       (1)),a1)*180/pi;
    angle_dev2 = shortest_angle_path(deg2rad(home_angle
       (2)),a2)*180/pi;

    cost_angle_change = a(1)*move1^2 + a(2)*move2^2;
    cost_thrust = b(1)*F1^2 + b(2)*F2^2;
    cost_thrust_change = c(1)*(F1-F1_last)^2 + c(2)*(F2
       -F2_last)^2;
    cost_angle_dev = d(1)*(angle_dev1)^2 + d(2)*(
       angle_dev2)^2;
    cost_thrust_dev = e(1)*(mean_thrust(1)-F1)^2 + e(2)
       *(mean_thrust(2)-F2)^2;
```

```
32
33      cost = cost_angle_change + cost_thrust +
           cost_thrust_change + cost_angle_dev +
           cost_thrust_dev;
34  end
```

Appendix C

Appended papers

This appendix contains the two scientific papers that make up the main contributions of the thesis.

C.1 Paper 1: Control allocation for double-ended ferries

This paper is a continuation of my project thesis work. The idea for this paper was formed while working with NTNUs autonomous passenger ferry prototype during a summer internship in 2018. The paper accepted for publication at the 2019 Control Applications for Marine Systems (CAMS) conference.

Control allocation for double-ended ferries with full-scale experimental results

Tobias R. Torben * **Astrid H. Brodtkorb** * **Asgeir J. Sørensen** *

* *Centre for Autonomous Marine Operations (NTNU AMOS), Department of Marine Technology, Norwegian University of Science and Technology (NTNU), Otto Nielsens vei 10, 7052 Trondheim, Norway (e-mail: tobias.torben@ntnu.no, astrid.h.brodtkorb@ntnu.no, asgeir.sorensen@ntnu.no)*

Abstract: A novel control allocation algorithm for double-ended ferries with symmetrical thruster configuration is proposed. The allocation problem is formulated using the extended thrust representation, resulting in a four dimensional constrained optimization problem. Using the thrust configuration constraint, the optimization problem is reduced to a scalar bounded optimization problem, for which there exists fast solvers. We propose a cost function and bounds such that the allocation algorithm supports the standard way of performing manual thruster control on ferries. A simulation study in conjunction with full-scale experimental results demonstrate the real-time performance of the proposed algorithm.

Keywords: Control allocation; Thrust allocation; Autonomous ferries; Nonlinear Optimization

1. INTRODUCTION

In the recent years there has been high activity related to autonomy in ferry operations, both in academia and in the industry (Torben, 2018; Bitar, 2017; Rolls-Royce Marine, 2018; Kongsberg Maritime, 2018). Due to the relatively low mission complexity, ferry operations make a good candidate for piloting the transition towards increased autonomy in ships.

Automating the navigation tasks requires new developments for high-level control. However, at the control execution level, functionality resembling a traditional dynamic positioning (DP) system must exist. The performance and robustness of the DP system is paramount for the success of the mission. For over-actuated marine vessels, control allocation is a vital part of the DP system. Improper allocation may lead to degraded control performance, lower energy efficiency, and increased wear and tear on the actuators.

In this paper, we treat control allocation for double-ended ferries with symmetrical thruster configuration. This is a standard setup for car ferries, of which there exists several hundred in Scandinavia. These ferries have one azimuth thruster in each end, as shown in Figure 2. A challenge with this configuration is that it may take considerable time to change the direction of thrust, as the turning rate of the azimuths is usually low. In particular, when a braking force is required, one thruster must turn 180 degrees. This time delay is unacceptable for high-precision maneuvers, such as docking. Also, if not treated carefully, the thruster may produce a force in the wrong direction while turning, which may have a destabilizing effect on the motion control system.

For manual thruster control, it is common to turn the front thruster 180 degrees when approaching the dock. A force can then quickly be produced in both forward and reverse direction by balancing the thrust on the two thrusters. At some ferry sites, turning the front thruster by 180° is restricted, as the thruster wake may cause erosion damage to the quay. In this case the aft thruster is turned instead. The principle is the same, however some thruster-thruster interactions may occur.

As far as the authors are aware, no previous published work exists for control allocation for double-ended ferries. However, there is a rich literature in control allocation for marine surface vessels, commonly referred to as *thrust allocation*. In-depth reviews of the literature are given in Fossen and Johansen (2006) and Johansen and Fossen (2013). Two methods dominate the literature. The Pseudo-inverse method (Sørdalen, 1997), and variations of the Quadratic Programming (QP) method (Ruth, 2008). The Pseudo-inverse method has an advantage in its simplicity and low computational complexity, but it yields an unconstrained solution, and also it does not support the thruster control method as experienced for manual thruster control. The strength of the QP method is that it can add both equality and inequality constraints. Drawbacks include relatively high computational complexity and the fact that the original allocation problem must be linearized before it can be formulated as a QP problem.

The main scientific contribution of this paper is the development of an efficient nonlinear control allocation algorithm. The algorithm uses the thrust configuration constraint to reduce the solution space, and is able to control the thrusters in a similar manner as described for manual

⋆ This work was supported by the Research Council of Norway through the Centres of Excellence funding scheme, project number 223254 - NTNU AMOS, and the KPN ORCAS project, project number 280655.

Fig. 1. The NTNU-developed, fully electric passenger ferry prototype, milliAmpere, used in the experimental testing. Photo: Kai T. Dragland

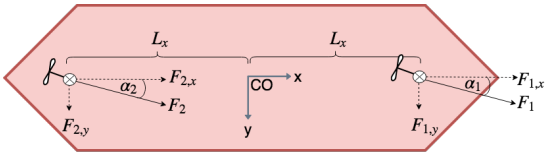

Fig. 2. Thruster configuration for double-ended ferries.

thruster control. The algorithm is tested in simulation and in full-scale experiments with the passenger ferry prototype milliAmpere, shown in Figure 1. The algorithm was developed for the NTNU Autoferry milliAmpere, and was first presented in Torben (2018).

The paper is organized as follows:

In Section 2 the problem formulation is described. In Section 3 we present the novel control allocation algorithm. In Section 4 we present and discuss the results from simulations and full-scale experiments. Conclusions are given i Section 5.

2. PROBLEM FORMULATION

In this paper we consider the control allocation problem for the thruster configuration shown in Figure 2. This figure also shows the definition of the symbols and directions used in this paper.

For marine vessels with the horizontal plane (surge, sway, yaw) as its working space, the input to the thrust allocation module is the desired body frame control action $\tau = [X, Y, N]^\top$. The output from the thrust allocation is the setpoints to the actuators. This can for instance be in form of propeller speed or pitch, engine torque or power, or rudder angle, depending on the type of actuator and the corresponding mapping of the desired force (Smogeli et al., 2005).

The mapping from actuator setpoints to body frame control action can be formulated as

$$\tau = B(\alpha)u \tag{1}$$

where α is a vector of unknown actuator angles and u is an unknown vector of control inputs. The matrix B is called the *thrust configuration matrix*. The objective of the control allocation problem is to find an inverse mapping, that is, determine u and α such that the resulting generalized force produced is τ. For over-actuated marine vessels, the system of (1) is under-determined, that is, there are infinitely many solutions. This gives the thrust allocation algorithm freedom to choose a combination of u and α that is optimal in some sense.

For azimuth thrusters, we can remove the dependence on α from B by considering the surge and sway components of the thrust produced from one actuator. This is referred to as the *extended thrust representation* (Sørdalen, 1997). In the case of n azimuth thrusters, (1) takes the form

$$\tau = Bu = \begin{pmatrix} 1 & 0 & \dots & 1 & 0 \\ 0 & 1 & \dots & 0 & 1 \\ -L_{1,y} & L_{1,x} & \dots & -L_{n,y} & L_{n,x} \end{pmatrix} \begin{pmatrix} F_{1,x} \\ F_{1,y} \\ \vdots \\ F_{n,x} \\ F_{n,y} \end{pmatrix} \tag{2}$$

where $L_{i,x}$ and $L_{i,y}$ are the distances from thruster i to the center origin (CO) in surge and sway directions, respectively. $F_{i,x}$ and $F_{i,y}$ are the surge and sway components of the thrust produced by thruster i.

From the thrust components, the thrust and azimuth angle for each thruster can easily be retrieved as follows:

$$F_i = \sqrt{F_{i,x}^2 + F_{i,y}^2}, \quad \alpha_i = \arctan \frac{F_{i,y}}{F_{i,x}} \tag{3}$$

In this paper we consider thrusters which can not reverse the thrust, since this is usually the case. However, it can be shown that the method can be extended to cover thrusters which can reverse the thrust as well.

3. NONLINEAR SCALAR CONTROL ALLOCATION

In this section we first develop the nonlinear scalar allocation algorithm, and then give some guidelines for choosing the bounds in the optimization problem and the cost function. Finally we summarize all the steps involved.

3.1 Transformation to a scalar, bounded optimization problem

When applying the extended thrust representation to the thruster configuration of Figure 2, the thrust configuration matrix, $B \in \mathbb{R}^{3\times 4}$, becomes

$$B = \begin{pmatrix} 1 & 0 & 1 & 0 \\ 0 & 1 & 0 & 1 \\ -L_{1,y} & L_{1,x} & -L_{2,y} & L_{2,x} \end{pmatrix} \tag{4}$$

By assigning the index 1 to the front thruster and 2 to the aft thruster, and exploiting the symmetry properties of double ended ferries, it is clear that $L_{1,y} = L_{2,y} = 0$ and $L_{1,x} = L_x = -L_{2,x}$. Applying this to (4) yields

$$B = \begin{pmatrix} 1 & 0 & 1 & 0 \\ 0 & 1 & 0 & 1 \\ 0 & L_x & 0 & -L_x \end{pmatrix} \tag{5}$$

A key observation here is that B is a Rank 3 matrix, whereas there are 4 unknown thrust components to be determined:

$$u = [F_{1,x}, F_{1,y}, F_{2,x}, F_{2,y}]^\top$$

Hence, there is in fact only one degree of freedom in the thrust mapping $\tau = Bu$. The main idea for the new thrust allocation algorithm is to reformulate the original optimization problem with 4 variables (7, if slack variables are used as in Johansen et al. (2004)) into a bounded scalar optimization problem in the one, free variable of the equation $\tau = Bu$.

To do this reformulation, the structure of the solution space of $\tau = Bu$ is investigated. First, the augmented matrix for the linear system is set up:

$$(\,B|\tau\,) = \begin{pmatrix} 1 & 0 & 1 & 0 & X \\ 0 & 1 & 0 & 1 & Y \\ 0 & L_x & 0 & -L_x & N \end{pmatrix} \tag{6}$$

Next, Gaussian elimination is performed on $(\,B|\tau\,)$ until the matrix is in reduced row echolon form. This yields the equivalent linear system of equations

$$\begin{pmatrix} 1\ 0\ 1\ 0 & X \\ 0\ 1\ 0\ 0 & \dfrac{N + L_x Y}{2L_x} \\ 0\ 0\ 0\ 1 & -\dfrac{N - L_x Y}{2L_x} \end{pmatrix} \tag{7}$$

Written in matrix-vector form, (7) becomes

$$\begin{pmatrix} 1\ 0\ 1\ 0 \\ 0\ 1\ 0\ 0 \\ 0\ 0\ 0\ 1 \end{pmatrix} \begin{pmatrix} F_{1,x} \\ F_{1,y} \\ F_{2,x} \\ F_{2,y} \end{pmatrix} = \begin{pmatrix} X \\ \dfrac{N + L_x Y}{2L_x} \\ -\dfrac{N - L_x Y}{2L_x} \end{pmatrix} \tag{8}$$

Multiplying out (8) and writing out the components yields:

$$F_{1,x} + F_{2,x} = X \tag{9a}$$

$$F_{1,y} = \frac{N + L_x Y}{2L_x} \tag{9b}$$

$$F_{2,y} = -\frac{N - L_x Y}{2L_x} \tag{9c}$$

This shows that $F_{1,y}$ and $F_{2,y}$ are uniquely determined, whereas in (9a) there is one degree of freedom. Natural choices for the parametrization of the solution space are $F_{1,x}$ or $F_{2,x}$. $F_{1,x}$ is chosen here.

Next, the idea is to search for an optimal solution by trying different choices of $F_{1,x}$. For each step of the optimization, a candidate $F_{1,x}$ is selected. From this, $F_{2,x}$, $F_{1,y}$ and $F_{2,y}$ can be calculated from (9a) - (9c) such that the thrust configuration constraint is satisfied. Now that all the thrust components are known, the thrust magnitude and angle for each thruster can be calculated from (3). Knowing the thrust magnitude and angle for each thruster, a cost function can be defined to penalize, for instance, large thrust magnitudes or large changes of azimuth angle. This shows that the value of a cost function for all possible solutions to (9a) - (9c) can be calculated by only varying $F_{1,x}$. Two great advantages are thus achieved:

(1) To search for the optimal solution, we only need to solve a *scalar* optimization problem.
(2) For every candidate solution, the thrust configuration constraint, $\tau = Bu$, is automatically satisfied. This removes the need for equality constraints in the optimization problem, and the optimization problem can then be reduced to a *bounded* optimization problem, where the only constraints are fixed bounds on $F_{1,x}$.

The reason why this is a great advantage, is that for scalar, bounded optimization problems, there exists fast and robust nonlinear solvers. Popular alternatives include Brent's Method (Brent, 1971) and Golden Section Search (Press et al., 1992). Two example implementations are MATLABs *fminbnd* and Python SciPys *fminbound*.

3.2 Choosing the bounds in the optimization problem

There are several options for choosing the bounds on $F_{1,x}$ in the optimization problem. First of all, the bounds should ensure that the allocation algorithm does not command a greater thrust than the thrusters can deliver. To ensure that a feasible solution exists for the optimization problem, the commanded control action, $\tau = [X, Y, N]^\top$, should also be saturated before entering the control allocation module. If it is desirable that the front is turned 180°, as described in Section 1, this can be achieved by constraining the front thruster to only produce a negative surge force, and the aft thruster to only produce a positive surge force.

To enforce these constraints, the requirement for the front thruster is that $F_{1,x} < 0$ and $F_{1,x} > -\sqrt{T_{max}^2 - F_{1,y}^2}$, where T_{max} is the maximum thrust produced by one thruster.

Similarly, the requirement for the aft thruster is that $F_{2,x} > 0$ and $F_{2,x} < \sqrt{T_{max}^2 - F_{2,y}^2}$. Since the variable of the optimization problem is $F_{1,x}$, these constrains must be expressed in terms $F_{1,x}$. This can easily be achieved using (9a). This gives that $F_{1,x} < X$ and $F_{1,x} > X - \sqrt{T_{max}^2 - F_{2,y}^2}$.

In the end, these constraints give two upper and two lower bound on $F_{1,x}$. The bounds used in the optimization problem are chosen to be the most restrictive of the two. This yields the bounds

$$F_{1,x}^{min} = \max(-\sqrt{T_{max}^2 - F_{1,y}^2}, X - \sqrt{T_{max}^2 - F_{2,y}^2}) \tag{10}$$

$$F_{1,x}^{max} = \min(0, X) \tag{11}$$

3.3 Choosing a cost function

In optimal control allocation algorithms, it is common to penalize the thrust magnitude, the change in thrust magnitude and the change in azimuth angle. As noted in Section 3.1, it is possible to evaluate these costs for all possible solutions by only varying $F_{1,x}$. Note that when the azimuth angles enter the cost function, it becomes nonlinear due to (3).

If the thruster control method where the front thruster is turned 180 degrees is used, the offset from the *home angles*, $\alpha_1 = 180°$, $\alpha_2 = 0°$, can also be penalized. When tuning the weights in the cost function, there is a trade-off between energy efficiency and control performance. If less weight is enforced on the angle change and deviation from home angle and more weight is enforced on the thrust usage and thrust change, the algorithm will allow the thrusters to have larger angular displacements. For a given commanded sway force or yaw moment, a lower thrust is then needed to produce it, since the thrust will have a larger lateral component. However, due to the low servo speed, this will also yield a larger delay from commanded forces to produced forces.

In manual thruster control during docking, it is also common to give both thrusters a mean thrust against each other. This yields even faster response from commanded to produced control action, since it removes much of the spin-up time. Of course, it will also increase the energy consumption since the thrusters are constantly counteracting each other. The control allocation algorithm can easily be extended to support this by adding a term in the cost function which penalizes deviations from a prescribed mean thrust.

Using all the ideas introduced in this section, the cost function can take the form

$$C(F_{1,x}, F_{1,y}, F_{2,y}, \tau, \alpha^-, T^-) = w_T \|T\| + w_{\Delta T} \|\Delta T\| + w_{\delta T} \|\delta T\| + w_{\delta\alpha} \|\delta\alpha\| + w_{\Delta\alpha} \|\Delta\alpha\| \tag{12}$$

where $\alpha^-, T^- \in \mathbb{R}^2$ are the azimuth angles and thrust magnitudes from last time step, and $T, \alpha \in \mathbb{R}^2$ are the thrust magnitudes and azimuth angles found from (3). $F_{2,x}$ is found from (9a). $\Delta\alpha \in \mathbb{R}^2$ are the shortest angle paths from α^- to α, $\delta\alpha \in \mathbb{R}^2$ are the shortest angle paths from α to the home angles. $\Delta T \in \mathbb{R}^2$ are the changes in thrust magnitude from last time step, and $\delta T \in \mathbb{R}^2$ are the deviations from the mean thrusts. $w_T, w_{\Delta T}, w_{\delta T}, w_{\Delta\alpha}, w_{\delta\alpha} \in \mathbb{R}_{\geq 0}$ are the corresponding weights.

3.4 Summary of the control allocation algorithm

To do one iteration of the nonlinear scalar allocation algorithm, the following steps must be performed:

(1) Input the desired control action, τ, and the thrust magnitudes and angles from last time step. Saturate the desired control action to ensure that a feasible solution exists.
(2) Set bounds on $F_{1,x}$ using, for instance, (10) and (11).
(3) Calculate $F_{1,y}$ and $F_{2,y}$ from (9b) and (9c).
(4) Formulate a cost function to minimize, for instance (12).
(5) Solve a nonlinear bounded scalar optimization problem where $F_{1,x}$ is the free variable and $F_{1,y}$, $F_{2,y}$, τ are constant parameters.
(6) Calculate $F_{2,x}$ from (9a).
(7) Calculate the thrust magnitude and azimuth angle setpoints from (3).

4. RESULTS AND DISCUSSION

To evaluate the performance of the novel control allocation algorithm, we use simulations in conjunction with experimental results. Simulations have the advantage that the produced thrust is known, and we can therefore compare the commanded and produced thrust. In experimental testing, the produced thrust is usually not known. Instead, we will evaluate the DP performance of the ferry when using the nonlinear scalar control allocation algorithm.

4.1 Simulation setup, results and discussion

In the simulation study, a simplified model for an azimuth thruster, which can not reverse the thrust, is used. The thruster dynamics are modelled as a saturated first order system:

$$\dot{T} = \frac{1}{\theta}(T_c - T) \tag{13a}$$

$$T = \max(0, \min(T_{max}, T)) \tag{13b}$$

where T is the produced thrust, T_c is the commanded thrust, T_{max} is the maximal thrust and θ is the thrust time constant.

The closed-loop azimuth servo is modelled as a proportional controller from angle offset to servo speed with saturation on the maximal servo speed. The dynamics of the servo is neglected, that is, the actual servo speed is assumed equal to the commanded servo speed.

$$\dot{\alpha} = r \tag{14a}$$

$$r = \max(-r_{max}, \min(r_{max}, -K_p(\alpha - \alpha_c))) \tag{14b}$$

where α is the actual azimuth angle, α_c is the commanded azimuth angle, r is the servo speed, r_{max} is the maximal servo speed and K_p is the proportional gain.

The commanded control action is generated stochastically from a first-order Gauss-Markov process (Fossen, 2011).

The implementation of the control allocation algorithm uses all the terms from (12). The parameters are given in Appendix A. For comparison, the Pseudo-inverse and QP methods are tested under the same conditions. The implementation of the QP method is that of Fossen and Johansen (2006), not including the singularity avoidance term.

Figure 3 shows the commanded generalized force, τ together with the actual produced generalized force, Bu, from the nonlinear scalar allocation algorithm. The results show good tracking in all degrees of freedom. Figure 4 shows the corresponding azimuth angles. The plot shows that both thrusters work in angles of $\pm 30°$ about their home angles. There is good compliance between commanded and actual azimuth angles, indicating that the allocation generates feasible references for the azimuth servos. Figure 5 shows the cumulative error between commanded and actual produced generalized force for the three allocation methods. The figure indicates better performance for the nonlinear scalar allocation algorithm, although this can not be claimed on this basis alone, since

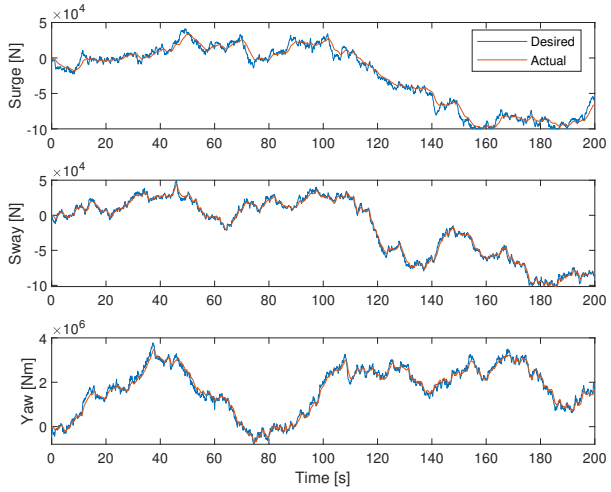

Fig. 3. Commanded and produced forces and moments for the nonlinear scalar control allocation algorithm.

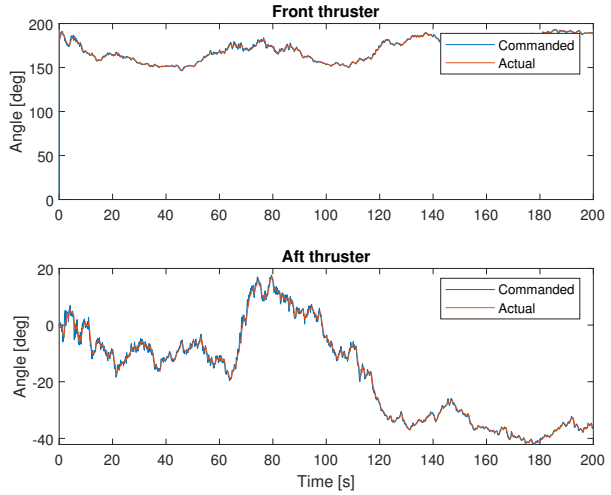

Fig. 4. Azimuth angles when using the nonlinear scalar control allocation algorithm.

there is a possibility of sub-optimal tuning for the QP method.

We have also compared the computational complexity to the Quadratic Programming (QP) method. In the comparison, we used the MATLAB *fminbnd* solver for the nonlinear scalar algorithm and the MATLAB *quadprog* solver for the QP method. Figure 6 shows histograms of elapsed time for one iteration. The nonlinear scalar allocation algorithm is, on average, 37.8 times faster. Also, it has a more narrow distribution. This is beneficial for robustness and predictability in a real-time control system.

4.2 Full-scale experimental setup results and discussion

The experimental tests were conducted with the passenger ferry prototype milliAmpere. Its main characteristics are given in Appendix B. The thrusters on this ferry can reverse the thrust, it is therefore not necessary to turn the front thruster 180°. The cost on deviation from home angle, deviation from mean thrust and the bounds

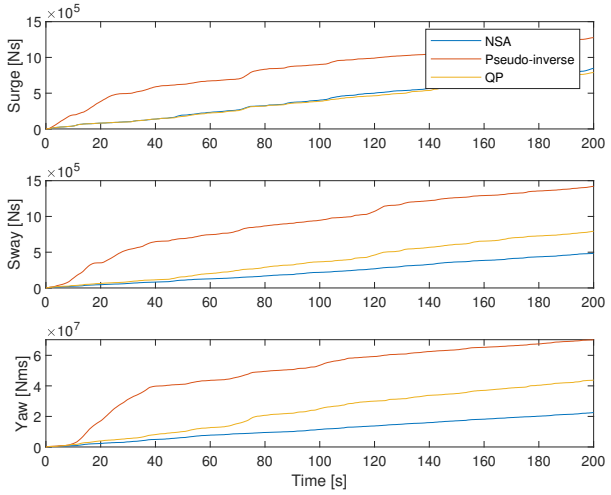

Fig. 5. Cumulative error for between commanded and produced generalized force for Nonlinear Scalar Allocation (NSA), Pseudo-inverse and QP

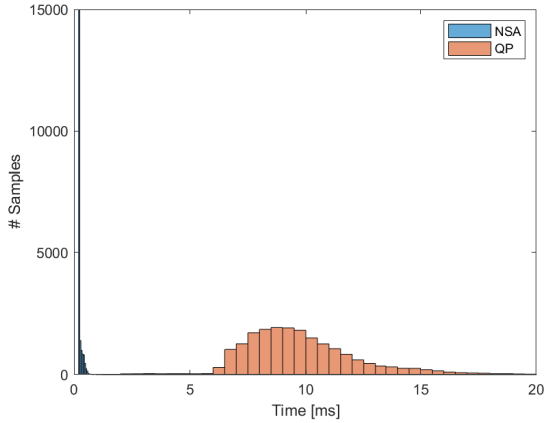

Fig. 6. Histogram of elapsed time for one iteration of NSA and QP for 20000 samples.

$F_{1,x} < 0$ and $F_{2,x} > 0$ was thus not used. We performed the commonly used 4-corner maneuver to evaluate the performance. The sides of the box are $10m$. The time used for one setpoint change is about $40s$. Between the each setpoint change, the ferry was performing stationkeeping for several minutes. In this way we test both transient and stationkeeping DP performance. The position and heading was obtained by Dual RTK GNSS, providing centimeter-level accuracy. The test was performed in calm conditions.

Figure 7 shows the trajectory for the 4-corner DP test. The figure shows good DP performance both in the transient and stationkeeping phases. DP performance is highly dependent on the performance of the control allocation. These results therefore give increased confidence for the feasibility of the novel control allocation algorithm for use in real-time DP control systems.

5. CONCLUSION

We have presented a novel control allocation algorithm for double-ended ferries with symmetrical thruster config-

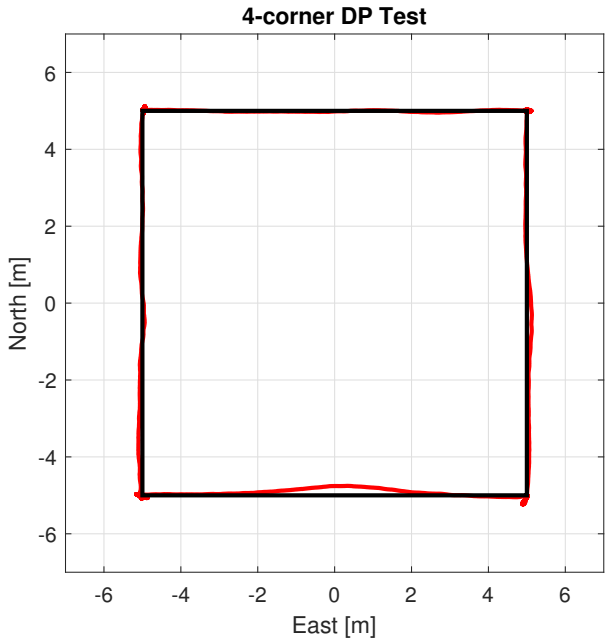

Fig. 7. Ferry trajectory from 4-corner DP test

uration. The algorithm reduces the dimension of solution space using the thrust configuration constraint, yielding a computationally efficient nonlinear optimization problem. Simulations and full-scale experimental results indicate promising real-time performance for use in a DP system.

ACKNOWLEDGEMENTS

The experimental testing was performed with funding from NTNU AMOS at the Autoferry project. Thanks to Brage Sæther for collaboration during testing.

REFERENCES

Bitar, G.I. (2017). *Towards the Development of Autonomous Ferries*. Master thesis, Department of Engineering Cybernetics. Norwegian University of Science and Technology (NTNU), Trondheim.

Brent, R.P. (1971). An algorithm with guaranteed convergence for finding a zero of a function. *The Computer Journal*, 14(4), 422–425. doi:10.1093/comjnl/14.4.422.

Fossen, T.I. (2011). *Handbook of Marine Craft Hydrodynamics and Motion Control*. Wiley.

Fossen, T.I. and Johansen, T.A. (2006). A survey of control allocation methods for ships and underwater vehicles. *14th Mediterranean Conference on Control and Automation, MED'06*, 1–6. doi:10.1109/MED.2006.328749.

Johansen, T.A. and Fossen, T.I. (2013). Control allocation - A survey. *Automatica*, 49(5), 1087–1103. doi:10.1016/j.automatica.2013.01.035.

Johansen, T.A., Fossen, T.I., and Berge, S.P. (2004). Constrained Nonlinear Control Allocation With Singularity Avoidance Using Sequential Quadratic Programming. *IEEE Transactions on Control Systems Technology*, 12(1), 211–216. doi:10.1109/TCST.2003.821952.

Kongsberg Maritime (2018). Teknologi til fremtidens ferger - Kongsberg Gruppen. URL `https://www.kongsberg.com/nb-no/kog/news/2018/april/teknologitilfremtidensferger/`.

Press, W.H., Teukolsky, S.A., Flannery, B., and Teukolsky, S. (1992). *Numerical Recipes in C*. doi:10.1097/SCS.0b013e318254359f.

Rolls-Royce Marine (2018). Press releases - Rolls-Royce and Finferries demonstrate world's first Fully Autonomous Ferry –Rolls-Royce. URL `https://www.rolls-royce.com/media/press-releases/2018/03-12-2018-rr-and-finferries-demonstrate-worlds-first-fully-autonomous-ferry.aspx`.

Ruth, E. (2008). *Propulsion control and thrust allocation on marine vessels*. Ph.D. thesis, NTNU.

Smogeli, N., Ruth, E., and Sørensen, A.J. (2005). Experimental validation of power and torque thruster control. *Proceedings of the 20th IEEE International Symposium on Intelligent Control, ISIC '05 and the 13th Mediterranean Conference on Control and Automation, MED '05*, 2005, 1506–1511. doi:10.1109/.2005.1469805.

Sørdalen, O.J. (1997). Optimal thrust allocation for marine vessels. *Control Engineering Practice*, 5(9), 1223–1231. doi:10.1016/S0967-0661(97)84361-4.

Torben, T.R. (2018). *Hybrid Control of Autonomous Ferries*. December. Project thesis, Department of Marine Technology. Norwegian University of Science and Technology (NTNU), Trondheim. doi:10.13140/RG.2.2.10564.88969.

Appendix A. PARAMETERS USED IN THE SIMULATIONS

Table A.1. Parameters for simulations

Description	Symbol	Value
Thrust time constant	θ	$2.0s$
Max thrust	T_{max}	$200kN$
Max servo speed	r_{max}	$10\frac{deg}{s}$
Servo proportional gain	K_p	$3.0\frac{1}{s}$
Distance from thruster to vessel center	L_x	$50m$
Mean thrust	T_{mean}	$50kN$
Weight on angle change	$w_{\Delta\alpha}$	10
Weight on thrust usage	w_T	0.1
Weight on thrust change	$w_{\Delta T}$	0.1
Weight on deviation from home angle	w_α	3
Weight on deviation from mean thrust	$w_{\delta T}$	0.1

Note: The weights in the cost function are for thrusts in kN and angles in degrees. The square of the norm is used instead of the norm in (12).

Appendix B. MAIN CHARACTERISTICS FOR MILLIAMPERE

Table B.1. milliAmpere main characteristics

Description	Symbol	Value
Length overall	LOA	$5.0m$
Beam	B	$2.8m$
Displacement	Δ	$1667kg$
Max thrust	T_{max}	$500.3N$

C.2 Paper 2: A resetting observer for LTV systems with applications to dynamic positioning of marine surface vessels

This paper is a continuation of a semester project in the PhD course MR8500. The topic for the course was hybrid dynamical systems. The work was initiated by an idea from Dr. Øivind K. Kjerstad and Professor Roger Skjetne for a resetting observer, which the author extended by introducing a finite-time observer approach. This is a draft paper to be submitted for publication at the 2020 American Control Conference (ACC).

A resetting observer for LTV systems with application to dynamic positioning of marine surface vessels

Tobias R. Torben * **Øivind K. Kjerstad** ** **Roger Skjetne** *

* *Centre for Autonomous Marine Operations (NTNU AMOS), Department of Marine Technology, Norwegian University of Science and Technology (NTNU), Otto Nielsens vei 10, 7052 Trondheim, Norway (e-mail: (tobias.torben, roger.skjetne)@ntnu.no)*
** *Kongsberg Maritime, Rasmus Rønnebergs gate 21, 6002, Ålesund, Norway (e-mail: oivind.kjerstad@km.kongsberg.com)*

Abstract: This paper presents a resetting observer for linear time-varying systems. The motivation for this is better handling of unmodelled dynamics and reactiveness to external disturbance without compromising steady-state performance. A reset is triggered if the output estimation error exceeds predefined bounds. The jump map for the reset uses a finite-time observer approach. The finite-time equations are derived for LTV systems, and a method for calculating the state transition matrices online is presented. The observer equations are formulated in a hybrid dynamical systems framework, and sufficient conditions for Uniform Global pre-Asymptotic Stability are given. The method is applied to observer design for dynamic positioning of marine surface vessels. Numerical simulations of this application show promising results, with improved transient performance.

Keywords: Observer; State Estimation; Finite-time observer; Hybrid systems; Dynamic positioning

1. INTRODUCTION

Observers play a vital role in many control systems. The main objective of an observer is to estimate the states of a system based on limited measurements. Also, an observer may have a signal processing role, where it filters noise and unwanted frequency components before the signal enters the control loop.

Dynamic Positioning (DP) of a marine vessel is the process of keeping its position and heading by use of its thrusters. Model-based observers are state-of-the-art in industrial DP systems. These observers are input only position and heading measurements, and estimate position, velocity and a force bias. In addition, a DP observer has a wave filtering function (Sørensen, 2011).

A challenge for DP observers is to handle unmodelled dynamics and external disturbances in a reactive manner, without using too high injection gains. This has the potential to improve the transient behaviour of the control system and may reduce fuel consumption. Several applications today call for DP systems able to more rapidly handle changing disturbances and transients. Examples include DP in ice, anchor handling operations and subsea pipe laying.

⋆ This work was supported by the Research Council of Norway through the Centres of Excellence funding scheme, project number 223254 - NTNU AMOS, and the KPN ORCAS project, project number 280655.

In the recent years, several observers and controllers to improve the transient DP performance have been proposed. An effective approach is to use velocity measurements in the observer. However, high-quality velocity measurements are not always available. The most common source of velocity measurement is the course and speed over ground from a GNSS receiver. These often give poor velocity measurements at low speed. Other approaches are implemented purely in software, and thus avoid the installation of expensive additional sensors. Examples include using time-varying observer gains (Vaerno et al., 2017), acceleration feedforward (Kjerstad and Skjetne, 2016), switching between a model-based and a signal based observer (Brodtkorb et al., 2018), and a resetting observer (Kjerstad, 2016). The latter has inspired the approach for this paper.

A method called *Finite-time observer* looks promising for calculating the estimated state after a reset. The concept is that for an observable linear time-invariant (LTI) system, two Luenberger observers can be designed. By comparing the outputs of these observers after some time, the exact system state can be calculated. Finite-time observers first appeared in the literature in (Engel and Kreisselmeier, 2002). Here, a continuous-time observer for an LTI system was developed using time-delays. Later, Raff and Allgöwer (2007) designed a finite-time observer for LTI systems that jumps the state estimate repeatedly after a fixed time interval.

In this paper, we examine a hybrid observer design with a resetting mechanism, where we enforce a jump in the state estimates if the estimation error exceeds a predefined bound. To calculate the new state estimates after a jump, a finite-time observer approach is used. The finite-time approach is extended to cover linear time-varying (LTV) systems, and an observer for a generic LTV system is developed. We then show how this observer can be applied for DP. To the authors best knowledge, no such observer has been developed before.

The paper is outlined as follows. The problem formulation is presented in Section 2. In Section 3, the novel observer equations are developed. In Section 4, a formal analysis is performed using hybrid systems theory. In Section 5 the resetting observer is applied to a DP system and results from numerical simulations are given. The present results are discussed in Section 6, before concluding remarks are given in Section 7.

2. PROBLEM FORMULATION

In this paper we consider LTV systems of the form

$$\dot{z} = A(t)z + B(t)u \tag{1}$$

$$y = C(t)z \tag{2}$$

with state $z \in \mathbb{R}^n$ and output $y \in \mathbb{R}^p$. The input $u \in \mathbb{R}^m$, and matrices $A(t) \in \mathbb{R}^{n\times n}$, $B(t) \in \mathbb{R}^{n\times m}$ and $C(t) \in \mathbb{R}^{p\times n}$ are piecewise continuous and bounded functions, and $(A(t), C(t))$ form an observable pair for each time $t \in [0, \infty)$. Under these conditions, a unique solution to (1)-(2) exists and is bounded for all time (Chen, 1999).

The objective is calculate a state estimate $\hat{z}$, knowing the input u, and given measurements of the output y.

3. RESETTING OBSERVER DESIGN

In this section we first derive how an exact state estimate for an LTV system can be obtained from two Luenberger observers, and then show how we can use this in a resetting observer.

3.1 Finite-time observer equations for LTV systems

Consider two Luenberger observers for (1)-(2) with state estimates z_1 and z_2:

$$\dot{z_i} = A(t)z_i + B(t)u + L_i(t)(y - C(t)z_i) \tag{3}$$

where $L_i(t) \in \mathbb{R}^{n\times p}$ is a piecewise continuous and bounded injection gain matrix, chosen such that $A_i(t) := A(t) - L_i(t)C(t)$ is Hurwitz for all $t \in [0, \infty)$.

Define the error variables $e_i = z - z_i$, such that

$$\dot{e_i} = \dot{z} - \dot{z_i} = A_i(t)e_i \tag{4}$$

The solution of this system can be expressed in terms of the state transition matrix Φ (Chen, 1999):

$$e_i(t) = \Phi_i(t, 0)e(0) \tag{5}$$

To calculate the true system state at time δ, the two observers are initialized with the same value. The initial estimation error $e(0)$ is thus equal for both observers. (5) can then be used to set up two vectorial equations with two unknowns, $e(0)$ and $z(\delta)$:

$$\Phi_1(\delta, 0)e(0) = z(\delta) - z_1(\delta) \tag{6}$$

$$\Phi_2(\delta, 0)e(0) = z(\delta) - z_2(\delta) \tag{7}$$

Solving (6) for $e(0)$ yields

$$e(0) = \Phi_1^{-1}(\delta, 0)(z(\delta) - z_1(\delta)) \tag{8}$$

Inserting this into (7) and solving for the true system state, $z(\delta)$ then yields

$$z(\delta) = (I - \Phi_2(\delta, 0)\Phi_1^{-1}(\delta, 0))^{-1} \begin{bmatrix} -\Phi_2(\delta, 0)\Phi_1^{-1}(\delta, 0) & I \end{bmatrix} \begin{bmatrix} z_1 \\ z_2 \end{bmatrix} \tag{9}$$

Hence, if $\Phi_1(\delta, 0)$ and $I - \Phi_2(\delta, 0)\Phi_1^{-1}(\delta, 0)$ are invertible matrices, the true system state can be calculated in terms of z_1 and z_2. This value can be used to update the state estimates after a jump.

3.2 Calculating the state transition matrices

For a generic LTV system, a closed-form expression of the state transition matrix rarely exists. Also, if the time-dependence is driven by an external signal, this may not be known in advance. Here, we show how the numerical state transition matrix can be calculated recursively in an observer.

For a generic LTV system, the zero-input response is given by

$$x(t) = \Phi(t, 0)x(0) \tag{10}$$

Differentiating both sides of (10) with respect to time yields

$$\dot{x}(t) = A(t)x(t) = A(t)\Phi(t, 0)x(0) = \dot{\Phi}(t, 0)x(0) \tag{11}$$

Hence, the state transition matrix is governed by the differential equation

$$\dot{\Phi}(t, 0) = A(t)\Phi(t, 0) \tag{12}$$

Also, $\Phi(0, 0) = I$, where $I \in \mathbb{R}^{n\times n}$ is the identity matrix. Therefore, the value of $\Phi(t, 0)$ can be calculated online by integrating (12) with initial condition $\Phi(0, 0) = I$.

3.3 Implementational considerations

Only the state estimate z_1 is used as an output of the observer. z_2 is only included to accommodate a finite-time jump map. A_1 should therefore be tuned less aggressively than A_2 to minimize the noise in the state estimates.

A jump is triggered only if the estimation error exceeds predefined bounds. Define the bounds $\epsilon \in \mathbb{R}^p_{>0}$. A jump is triggered if $|(y - C(t)z_1)_i| \geq \epsilon_i$ for some $i \in [1, 2, ..., p]$.

Because a non-aggressive observer is used during steady-state conditions, and a jump is triggered only in the

transient of a disturbance, this design gives the observer a "low gain - high reactivity" property, which is desired in observers.

For a practical implementation of this observer, some modifications are necessary. There needs to be some control of the jump timing. The determinant of $I - \Phi_2(t,0)\Phi_1^{-1}(t,0)$ will tend to zero as $t \to 0$, which gives numerical issues when calculating its inverse. This is not surprising, as the two Luenberger observers must run for some time for us to extract information about the true system state from them. Because of this, two consecutive jumps must be separated by some dwell-time.

Also, the integral for the state transition matrices of (12) should be reset if the system flows for a long period of time. (9) includes the term $\Phi_1^{-1}(\delta, 0)$. Inverting a state transition matrix results in solving the LTV system backwards in time. Since A_1 is a Hurwitz matrix, this inverse will therefore grow exponentially in time. This would be problematic for implementation in a digital computer, if the observer was allowed to flow indefinitely. Also, modelling errors may cause drift in the state transition matrices if they are integrated over long time periods.

To control the timing of the jumps, we propose to always reset the state transition integrals after some constant time δ. The state transition matrices are reset to identity and z_2 is reset to the value of z_1. A jump in z_1 is triggered only if $|(y - C(t)z_1)_i| \geq \epsilon_i$ for some $i \in [1, 2, ..., p]$. If not, z_1 is kept unchanged after the reset.

Finally, to give a tunable aggressiveness of the jumps, a linear interpolation is added to the jump map. That is, instead on jumping directly to the z value dictated by (9), the system jumps to a value between the current estimate, z_1, and and z.

The complete observer equations are formulated in a hybrid systems framework in Section 4.

4. FORMAL ANALYSIS

4.1 Preliminaries from Hybrid Dynamical Systems theory

To formulate the observer equations and do a formal analysis, the framework of Goebel et al. (2012) is used. Only the main concepts and the results needed in our analysis is presented here. The reader is referred to (Goebel et al., 2012) and references therein for further details.

In this framework, a hybrid dynamical system, $\mathcal{H} = (C, F, D, G)$, is modelled as a *constrained differential inclusion* and a *constrained difference inclusion*:

$$x \in C \quad \dot{x} \in F(x) \tag{13a}$$

$$x \in D \quad x^+ \in G(x) \tag{13b}$$

When the state x is in the *flow set* C, it *flows* according to the *set-valued mapping* $\dot{x} = f(x)$ for some $f \in F$. When x is in the *jump set* D, it *jumps* according to set-valued mapping $x^+ = g(x)$ for some $g \in G$. x^+ denotes the value of x after a jump.

A special class of hybrid systems are *well-posed hybrid systems*. For these systems there exists an extensive toolbox of stability and robustness results. Sufficient conditions for $\mathcal{H} = (C, F, D, G)$ to be well-posed are provided by the *Hybrid Basic Conditions* (Goebel et al. (2012), Assumption 6.5):

- C and D are closed subsets of $\mathbb{R}^n$.
- $F : \mathbb{R}^n \rightrightarrows \mathbb{R}^n$ is outer semicontinuous and locally bounded relative to C, $C \subset dom(F)$, and $F(x)$ is a convex set for every $x \in C$.
- $G : \mathbb{R}^n \rightrightarrows \mathbb{R}^n$ is outer semicontinuous and locally bounded relative to D, and $D \subset dom(G)$.

Next, a hybrid Lyapunov theorem, which gives sufficient conditions for uniform global pre-asymptoptic stability (UGpAS) of a closed set, is stated. The theorem is a relaxed version of Goebel et al. (2012) Theorem 3.18, where it allows non-decrease in the Lyapunov function during jumps if the duration of flow is sufficiently large.

Theorem 1. *Sufficient Lyapunov Conditions; Persistent Flowing (Goebel et al. (2012) Proposition 3.27)*
Let $\mathcal{H} = (C, F, D, G)$ be a hybrid system and let $\mathcal{A} \subset \mathbb{R}^n$ be closed. Suppose V is a Lyapunov function candidate for $\mathcal{H}$ and there exist $\alpha_1, \alpha_2 \in \mathcal{K}_\infty$ and a continuous $\rho \in \mathcal{PD}$ such that

$$\alpha_1(\|x\|_{\mathcal{A}}) \leq V(x) \leq \alpha_2(\|x\|_{\mathcal{A}}) \quad \forall x \in C \cup D \cup G(D) \tag{14a}$$

$$\langle \nabla V(x), f \rangle \leq -\rho(\|x\|_{\mathcal{A}}) \quad \forall x \in C, f \in F(x) \tag{14b}$$

$$V(g) - V(x) \leq 0 \quad \forall x \in D, g \in G(x) \tag{14c}$$

If, for each $r > 0$, there exists $\gamma_r \in \mathcal{K}_\infty$, $N_r > 0$ such that for every solution ϕ to $\mathcal{H}$, $\|\phi(0,0)\|_{\mathcal{A}} \in (0, r]$, $(t, j) \in dom(\phi)$, $t + j \geq T$ imply $t \geq \gamma_r - N_r$, then $\mathcal{A}$ is uniformly globally pre-asymptotically stable for $\mathcal{H}$.

The term of *pre-asymptotic* as opposed to asympotic stability and *pre-attraction* as opposed to attraction indicates the possibility of a maximal solution that is not complete.

For systems satisfying the hybrid basic conditions, UGpAS also implies robust UGpAS. This ensures that vanishing perturbations do not dramatically change the behaviour of solutions.

4.2 Hybrid observer equations

We are now ready to state the hybrid observer equations for the resetting observer. To prove UGpAS, we first define a more general system which satisfies the hybrid basic conditions. All solutions for our resetting observer are contained in the set of solutions for this system. UGpAS for the observer therefore follows from UGpAS of this system.

The state of the hybrid system is defined as

$$x = (z, z_1, z_2, \Phi_1, \Phi_2, \zeta, \tau) \in N \times \mathbb{R}^n \times \mathbb{R}^n \times M \times M \times \mathbb{R}_{\geq 0} \times \mathbb{R}_{\geq 0} \tag{15}$$

where z is the true system state, which is assumed to live in a compact set $N \subset \mathbb{R}^n$, z_1 and z_2 are the Luenberger state estimates, and Φ_1 and Φ_2 are the state transition matrices. The latter are governed by (12), and will thus have no finite escape times. Also, since they are periodically reset to identity, these matrices will live in a compact set $M \subset \mathbb{R}^{n \times n}$. ζ and τ are scalar timer variables.

Following the developments of Section 3, the flow map and jump map may now be expressed as

$$\dot{x} = f(x) = \begin{bmatrix} A(\tau)z + B(\tau)u \\ A_1(\tau)z_1 + B(\tau)u + (A(\tau) - A_1(\tau))z \\ A_2(\tau)z_2 + B(\tau)u + (A(\tau) - A_2(\tau))z \\ A_1(\tau)\Phi_1 \\ A_2(\tau)\Phi_2 \\ 1 \\ 1 \end{bmatrix} \quad (16)$$

$$x^+ \in G(x) = \begin{bmatrix} z \\ \{KJ(x) + (I-K)z_1, z_1\} \\ \{KJ(x) + (I-K)z_1, z_1\} \\ I \\ I \\ 0 \\ \tau \end{bmatrix} \quad (17)$$

where $J(x) = (I - \Phi_2\Phi_1^{-1})^{-1}\begin{bmatrix}-\Phi_2\Phi_1^{-1} & I\end{bmatrix}\begin{bmatrix}z_1 \\ z_2\end{bmatrix}$, and K is a diagonal gain matrix with $0 < k_{ij} < 1$.

For the resetting observer, z_1 and z_2 jump to either $z_1 + K(J(x) - z_1)$ or z_1 based on whether the output estimation error exceeds the ϵ bounds or not. This conditional would yield a jump map that is not outer semicontinuous, and therefore a hybrid system that does not satisfy the hybrid basic conditions. This is overcome by using a set-valued mapping that contains both values in the jump map.

The flow set is defined as

$$C = N \times \mathbb{R}^n \times \mathbb{R}^n \times M \times M \times [0, \delta] \times \mathbb{R}_{\geq 0} \quad (18)$$

And the jump set is defined as

$$D = N \times \mathbb{R}^n \times \mathbb{R}^n \times M \times M \times \delta \times \mathbb{R}_{\geq 0} \quad (19)$$

4.3 Stability and well-posedness

In this section we show that the hybrid system of (16)-(19) satisfies the hybrid basic conditions, and give sufficient conditions for UGpAS of a closed set.

First we note that C and D are closed sets. $F = f(x)$ is locally bounded, outer semicontinuous and has convex values for every $x \in C$ by virtue of being a singleton set-valued mapping containing only a continuous function. Similarly $G(x)$ is locally bounded and outer semicontinuous for every $x \in D$. Continuity of $J(x)$ follows from the fact that the matrix inverse is a continuous function for non-singular matrices, and that continuity is conserved through products, sums and compositions with other continuous functions. This shows that the system of (16)-(17) satisfies all the hybrid basic conditions and, therefore, constitutes a well-posed hybrid system.

The following stability results provides sufficient conditions for the state estimate z_1 to converge asymptotically to z.

Theorem 2. *The set $\mathcal{A} = \{N \times \mathbb{R}^n \times \mathbb{R}^n \times M \times M \times [0, \delta] \times \mathbb{R}_{\geq 0} : z = z_1\}$ is UGpAS for (16)-(19) if Φ_1 and $(I - \Phi_2\Phi_1^{-1})$ are non-singular $\forall t > 0$, and there exists a Lyapunov function candidate for the continuous-time error dynamics, $\dot{e} = A_1(t)e$, which satisfies*

$$\alpha_1(\|e\|) \leq V(e,t) \leq \alpha_2(\|e\|) \quad (20a)$$

$$\langle \nabla V(e,t), f \rangle \leq -\rho(\|e\|) \quad (20b)$$

$$V((I-K)e, t) - V(e,t) \leq 0 \quad (20c)$$

for all times $t > 0$, where α_1, $\alpha_2 \in \mathcal{K}_\infty$ and $\rho \in \mathcal{PD}$.

Proof. First we note that $\|x\|_{\mathcal{A}} = \|z - z_1\| = \|e\|$ since z_2, Φ_1, Φ_2, ζ and τ are always in $\mathcal{A}$, by construction.

We also note that the time, t, in Equation (20) can be replaced by the timer state, τ, in the hybrid system. We can thus analyze stability of an unbounded set for a time-invariant hybrid system using Theorem 1.

Since $\|x\|_{\mathcal{A}} = \|e\|$, the assumptions of equation (14a) and (14b) are satisfied by (20a) and (20b), respectively.

Next, we note that

$$e^+ = e$$

or

$$e^+ = z^+ - z_1^+ = z - (z_1 + K(J(x) - z_1))$$

In the first case, $V(x^+) - V(x) = 0$, and (14c) is satisfied. In the second case, if Φ_1 and $(I - \Phi_2\Phi_1^{-1})$ are non-singular, then $J(x) = z$, as shown in Section 3.1. Then we have

$$e^+ = z - (z_1 + K(z - z_1)) = (I - K)e$$

Hence, (14c) is satisfied under the requirement of (20c).

What remains is to show that the duration of flow is sufficiently large to compensate for the non-decrease in the Lyapunov function during jumps.

Since a jump always occurs every δ time units we have that

$$j = \lfloor \frac{t}{\delta} \rfloor \leq \frac{t}{\delta} \implies t \geq \delta j$$

Adding δt to both sides of the inequality gives

$$\delta t + t \geq \delta j + \delta t \implies t(1+\delta) \geq \delta(t + j)$$

Solving for t finally yields

$$t \geq \frac{\delta}{1+\delta}(t + j)$$

Choosing $\gamma_r(T) = \frac{\delta}{1+\delta}T \in \mathcal{K}_\infty$ and $N_r = 0$ the condition of Theorem 1 is satisfied for every $r > 0$.

Together, this shows that the conditions of this theorem are sufficient to conclude UGpAS of $\mathcal{A}$ for (16)-(19). □

If the continuous-time dynamics, $\dot{e} = A_1 e$, is UGAS (or equivalently UGES), there always exists a quadratic, time-varying Lyapunov function which satisfies conditions (20a) and (20b) (Khalil, 2002). The following corollary is a special case of Theorem 2 when using a quadratic Lyapunov function.

Corollary 1. *The set $\mathcal{A} = \{N \times \mathbb{R}^n \times \mathbb{R}^n \times M \times M \times [0, \delta] \times \mathbb{R}_{\geq 0} : z = z_1\}$ is UGpAS for (16)-(19) if Φ_1 and $(I - \Phi_2\Phi_1^{-1})$ are non-singular $\forall t > 0$, and there exists a quadratic Lyapunov function, $V(e,t) = e^\top P(t)e$, for the continuous-time error dynamics, $\dot{e} = A_1(t)e$, which satisfies (20a) and (20b) and in addition*

$$\sqrt{\frac{\lambda_{min}(P(t))}{\lambda_{max}(P(t))}} \geq 1 - \min(K), \quad \forall t \quad (21)$$

Proof. Using Theorem 2, the only thing that remains to show is that (20c) holds.

Again we have that $e^+ = e$ or $e^+ = (I - K)e$.

In the first case, $V(e^+,t) - V(e,t) = 0$.

In the second case it follows that

$$\begin{aligned} &V(e^+,t) - V(e,t) \\ &= ((I-K)e)^\top P(I-K)e - e^\top Pe \\ &\leq \lambda_{max}(P)\left\|(I-K)e\right\|^2 - \lambda_{min}(P)\left\|e\right\|^2 \\ &\leq (1-min(K))^2\lambda_{max}(P)\left\|e\right\|^2 - \lambda_{min}(P)\left\|e\right\|^2 \end{aligned}$$

This shows that (20c) is satisfied under the requirement that $\sqrt{\frac{\lambda_{min}(P(t))}{\lambda_{max}(P(t))}} \geq 1 - \min(K) \quad \forall t.$ □

Remark 1. *Engel and Kreisselmeier (2002) give sufficient conditions for $(I - \Phi_2\Phi_1^{-1})$ to be non-singular in the time-invariant case:*

$(I - \Phi_2\Phi_1^{-1})$ is non-singular if there exists a $\sigma < 0$ such that the real part of all eigenvalues of A_1 are smaller than σ and the real part of all eigenvalues of A_2 are larger than σ.

5. CASE STUDY: DYNAMIC POSITIONING

The resetting observer of (16)-(19) applies to generic observable LTV systems. In this section we show how it can be applied in a DP system.

5.1 Mathematical modelling and observer design

The state-of-the-art control plant model used in observer design for DP is given by (Fossen and Strand, 1999):

$$\dot{\xi} = A_w\xi \tag{22a}$$
$$\dot{\eta} = R(\psi)\nu \tag{22b}$$
$$\dot{b} = -T_b^{-1}b \tag{22c}$$
$$M\dot{\nu} + D\nu = \tau + R^\top(\psi)b \tag{22d}$$
$$y = \eta + C_w\zeta \tag{22e}$$

where $\xi \in \mathbb{R}^6$ are the states of a second-order harmonic oscillator, modelling the wave frequency motion of the vessel, $\eta \in \mathbb{R}^3$ is the position and heading, $\nu \in \mathbb{R}^3$ is the body frame velocity and turn rate, $b \in \mathbb{R}^3$ is a bias term and $\tau \in \mathbb{R}^3$ is the body frame thruster forces. $A_w \in \mathbb{R}^{6\times6}$ is the state space matrix for a second order harmonic oscillator, $R(\psi) \in \mathbb{R}^{3\times3}$ is a three degree of freedom rotation matrix, $T_b \in \mathbb{R}^{3\times3}$ is a diagonal matrix of bias time constants, $M \in \mathbb{R}^{3\times3}$ is the mass matrix, including added mass, and $D \in \mathbb{R}^{3\times3}$ is the linear damping matrix.

Preliminary results showed difficulty in applying the finite-time methodology to the system of (22). The model used hereafter will therefore be a simplification of this model, where the wave-frequency model is not included. The intention of the wave-frequency model is to separate the wave-frequency motion and low-frequency motion. This is necessary because it is not desired that the wave-frequency components of the state estimates enter the control loop. In the model used hereafter, it is therefore necessary to add a notch-filter before the measurements enters the observer.

The modified low-frequency model is given by:

$$\dot{\eta} = R(\psi)\nu \tag{23a}$$
$$\dot{b} = -T_b^{-1}b \tag{23b}$$
$$M\dot{\nu} + D\nu = \tau + R^\top(\psi)b \tag{23c}$$
$$y = \eta \tag{23d}$$

Note that this is a nonlinear model due to the rotation matrices. However, if we use the heading measurements directly in the rotation matrices, setting $R(t) := R(\psi(t))$, this can be considered as an external time-varying signal. The observer can then be written in LTV form:

$$z = \left[\eta^\top, b^\top, \nu^\top\right]^\top \in \mathbb{R}^9, \quad u = \tau \in \mathbb{R}^3 \tag{24a}$$
$$\dot{z} = A(t)z + Bu \tag{24b}$$
$$y = Cz \tag{24c}$$

where

$$A(t) = \begin{bmatrix} 0_{3\times3} & 0_{3\times3} & R(t) \\ 0_{3\times3} & -T_b^{-1} & 0_{3\times3} \\ 0_{3\times3} & M^{-1}R(t)^\top & -M^{-1}D \end{bmatrix}$$

$$B = \begin{bmatrix} 0_{3\times3} \\ 0_{3\times3} \\ M^{-1} \end{bmatrix}$$

$$C = [I_{3\times3}\ 0_{3\times3}\ 0_{3\times3}]$$

Luenberger observers for z_1 and z_2 can then be designed as

$$\dot{z}_i = A(t)z_i + Bu + L_i(t)(y - Cz_i) \tag{25}$$

where

$$L_i(t) = \begin{bmatrix} K_1 \\ K_2 \\ M^{-1}R^\top(t)K_3 \end{bmatrix} \in \mathbb{R}^{9\times3}$$

such that $A_i(t) = A(t) - L_i(t)C$ is Hurwitz for all t.

These Luenberger observers can now readily be used in the resetting observer of (16)-(19).

5.2 Results from numerical simulations

To evaluate the performance of the proposed observer design, it was tested in simulation with a high-fidelity simulation model of an offshore supply vessel. We are mainly interested in its ability to handle rapidly changing loads, as discussed in Section 1. To this end, the vessel was excited by an impulsive sway disturbance at $t = 50s$. The vessel was first simulated in calm sea conditions, and then in a sea state governed by a JONSWAP wave spectrum. There is no position controller in the loop, so the observer-controller interactions are not addressed in this simulation study. All measurements are subject to additive Gaussian white noise. For the simulation in waves, the measurements were wave filtered before entering the observer. The parameters used in the simulations are given in Appendix A. The results are presented in Figures 1 and 2.

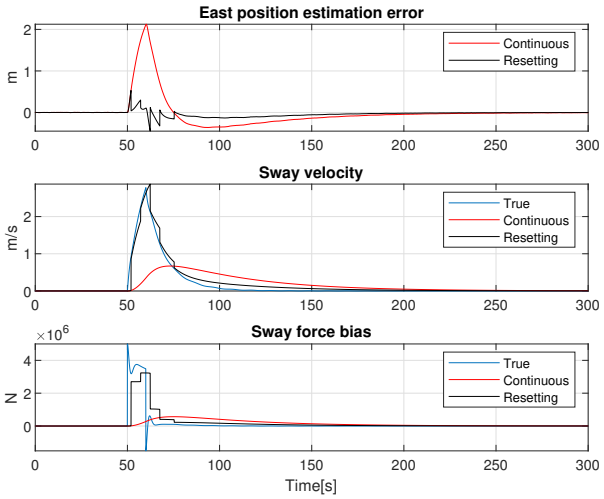

Fig. 1. Simulation results for DP observer in calm sea.

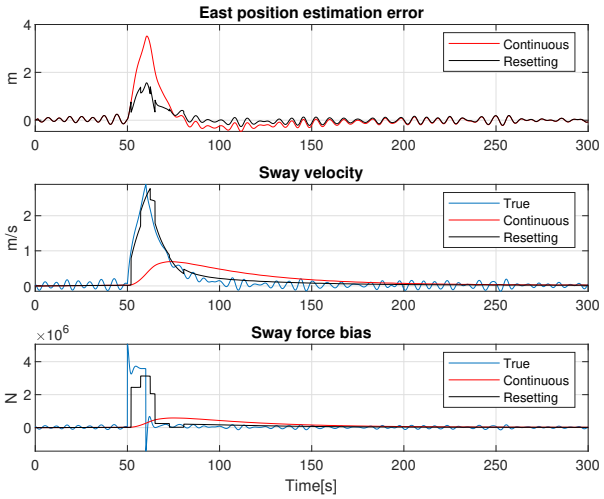

Fig. 2. Simulation results for DP observer in waves.

6. DISCUSSION

The results from the numerical simulations show promising performance. The resetting observer gave a substantial improvement during the transient phase, without amplifying measurements noise or introducing wave frequency components to the state estimates.

In the theoretical foundation, there are issues that needs addressing. We have given sufficient conditions for asymptotic stability. However, these results are likely very conservative. In fact, we were not able to find a Lyapunov function to satisfy the jump conditions of Theorem 2 for the DP case study, except for the trivial case of $K = I$. Finding relaxed conditions is thus a key topic for future research.

Also, conditions to ensure non-singularity of $(I - \Phi_2\Phi_1^{-1})$ for all times, and all variations of the external time-varying signal should be investigated. Menold et al. (2013) proposes a workaround for this problem for uniformly observable systems. Here, the system is transformed to observability canonical form. The time-varying parts of the dynamics are then separated out and cancelled in the observer, resulting in time-invariant error dynamics. This may be a good approach for some systems. However, for the DP case, the transformation requires knowledge of the turn rate and yaw acceleration. Since these signals are usually not available in a ship control system, this is not an attractive solution here. A practical solution to avoid inverting a singular matrix may be to add a check on the condition number of $(I - \Phi_2\Phi_1^{-1})$ before doing a jump.

7. CONCLUSION

We have presented a resetting observer for linear time-varying systems. A reset is triggered if the output estimation error exceeds predefined bounds. The jump map for the reset uses a finite-time observer approach. The finite-time equations has been derived for LTV systems, and a method for calculating the state transition matrices online has been presented. The observer equations has been formulated in a hybrid dynamical systems framework, and sufficient conditions for Uniform Global pre-Asymptotic Stability have be given.

The method has applications to observer design for dynamic positioning of marine surface vessels. A case study for this application was conducted with numerical simulations. The simulations showed promising results, with improved transient performance, compared to the state-of-the-art continuous-time observer.

The discussion highlights the need for further developments in the theoretical foundation. In particular, relaxed stability conditions and methods to guarantee non-singularity in the jump map are key topics for future research.

REFERENCES

Brodtkorb, A.H., Værnø, S.A., Teel, A.R., Sørensen, A.J., and Skjetne, R. (2018). Hybrid controller concept for dynamic positioning of marine vessels with experimental results. *Automatica*, 93, 489–497. doi:10.1016/j.automatica.2018.03.047. URL `https://doi.org/10.1016/j.automatica.2018.03.047`.

Chen, C.T. (1999). *Linear System Theory and Design*. Oxford University Press, third edition. doi:10.1016/0005-1098(86)90039-7.

Engel, R. and Kreisselmeier, G. (2002). A Continuous-Time Observer Which Converges in Finite Time. *IEEE Transactions on Automatic Control*, 47(7), 1202–1204. doi:10.1109/TAC.2002.800673.

Fossen, T.I. and Strand, J.P. (1999). Passive nonlinear observer design for ships using Lyapunov methods. *Automatica*, 35, 3–16.

Goebel, R., Sanfelice, R.G., and Teel, A.R. (2012). *Hybrid Dynamical Systems : Modeling, Stability, and Robustness*. Princeton University Press.

Khalil, H.K. (2002). Nonlinear Systems.

Kjerstad, Ø.K. (2016). *Dynamic Positioning of Marine Vessels in Level Ice*. Ph.D. thesis, NTNU.

Kjerstad, Ø.K. and Skjetne, R. (2016). Disturbance Rejection by Acceleration Feedforward for Marine Surface Vessels. *IEEE Access*, 4, 2656–2669. doi:10.1109/ACCESS.2016.2553719.

Menold, P.H., Findeisen, R., and Allgower, F. (2013). Finite time convergent observers for linear time-varying systems. *Proceedings of the 11th Mediterranean conference on control and automation (T7-078)*, (December), 5673–5678.

Raff, T. and Allgöwer, F. (2007). An impulsive observer that estimates the exact state of a linear continuous-time system in predetermined finite time. *2007 Mediterranean Conference on Control and Automation, MED*, (2), 2–4. doi:10.1109/MED.2007.4433909.

Sørensen, A.J. (2011). A survey of dynamic positioning control systems. *Annual Reviews in Control*, 35(1), 123–136. doi:10.1016/j.arcontrol.2011.03.008.

Vaerno, S.A., Brodtkorb, A.H., Skjetne, R., and Calabro, V. (2017). Time-varying model-based observer for marine surface vessels in dynamic positioning. *IEEE Access*, 5, 14787–14796. doi:10.1109/ACCESS.2017.2731998.

Appendix A. SIMULATION PARAMETERS

Parameter	**Value**
Vessel Lpp	$82.8m$
Vessel mass	$6362t$
Disturbance magnitude	$5 \times 10^6 N$
Disturbance duration	$10s$
Significant wave height	$2.0m$
Peak wave frequency	$1.0rad/s$
Position measurement noise variance	$10^{-5}m^2$
Heading measurement noise variance	$10^{-7}rad^2$
Reset time	$2.5s$

Tobias Rye Torben

Control allocation and observer design for autonomous ferries

NTNU
Norwegian University of
Science and Technology